WORKING PAPER Nº IDB-WP-1785

Powering Through Drought

The Impact of Water Scarcity on Electricity Generation

Lisa Bagnoli
Lenin H. Balza
José Belmar
David Matías

Inter-American Development Bank
Infrastructure and Energy Sector

December 2025

Powering Through Drought

The Impact of Water Scarcity on Electricity Generation

Lisa Bagnoli*
Lenin H. Balza*
José Belmar*
David Matías**

* Inter-American Development Bank
** Rice University

Inter-American Development Bank
Infrastructure and Energy Sector

December 2025

Cataloging-in-Publication data provided by the
Inter-American Development Bank
Felipe Herrera Library
Powering through drought: the impact of water scarcity on electricity generation / Lisa Bagnoli, Lenin H. Balza, José Belmar, David Matías.
p. cm. — (IDB Working Paper Series; 1785)
Includes bibliographical references.
1. Power resources-Effect of drought on-Chile. 2. Electric power production-Effect of drought on-Chile. 3. Greenhouse gas mitigation-Chile. I. Bagnoli, Lisa. II. Balza, Lenin. III. Belmar, José. IV. Matías, David. V. Inter-American Development Bank. Energy Division. VI. Series.
IDB-WP-1785

JEL Codes: Q54, Q41, Q25, O54.
Keywords: Droughts, Hydropower Generation, Thermal Generation, Electricity Systems, Emissions, Latin America and the Caribbean.

http://www.iadb.org

Contact information: leninb@iadb.org

Powering Through Drought: The Impact of Water Scarcity on Electricity Generation*

Lisa Bagnoli Lenin H. Balza José Belmar David Matías

December 4, 2025

Abstract

Changing weather patterns pose a fundamental challenge to electricity systems reliant on water resources. Using two decades of plant-level generation and fuel input data matched to hydrological basins in Chile, we show that local droughts reduce hydro output by about 25% on average and trigger sharp increases in thermal generation among plants with spare capacity. This substitution cushions short-run losses in supply and guarantees reliability of the system but creates a double burden for affected regions, which face both water scarcity and increases in local pollution. Emissions from high-capacity thermal plants rise by roughly 34% during system-wide droughts, corresponding to about 1.4–1.8% of annual national emissions and 5.5–6.5% of the power sector's total. We also document that prolonged droughts were followed by expansions in thermal capacity, consistent with long-run lock-in of high-carbon-intensity technologies. Together, these results provide quantitative benchmarks for infrastructure planning, highlight the risk of path dependence in investment under climatic stress, and underscore the importance of ensuring sufficient capacity, diversification, and resilience in power system planning.

JEL Codes: Q54, Q41, Q25, O54.
Keywords: Droughts, Hydropower Generation, Thermal Generation, Electricity Systems, Emissions, Latin America and the Caribbean.

*Bagnoli: Inter-American Development Bank, Infrastructure and Energy Sector (lbagnoli@iadb.org); Balza: Inter-American Development Bank, Infrastructure and Energy Sector (leninb@iadb.org); Belmar: Inter-American Development Bank, Infrastructure and Energy Sector (jbel@iadb.org); Matias: Rice University (em127@rice.edu). The views expressed herein are entirely those of the authors and do not necessarily reflect the views of the Inter-American Development Bank, its Board of Directors, or the countries they represent. The authors gratefully acknowledge support from the Inter-American Development Bank through its Economic and Sector Work Program (RG-E1915). We thank Clara Pasman for thorough research assistance at early stages of the project, Julio Acuña, Arturo Alarcón, Laura Heras, José Manuel Eguiguren, Carolina Tojal, and attendees of the INE Seminar for their comments and suggestions. Any errors are our own responsibility.

1 Introduction

Changing weather patterns pose a growing threat to global electricity systems because of shifts in general climatic conditions and natural resource availability and the increasing frequency and severity of extreme weather events. Among these, droughts are particularly disruptive, constraining generation capacity and undermining system reliability (International Energy Agency, 2021b). As water scarcity intensifies across many regions, electricity systems must cope with both immediate operational constraints and longer-term adaptation challenges that could reshape their structure and emissions trajectories.

Hydropower, which supplied more than 15% of global electricity in 2022, is especially vulnerable, as droughts affects both seasonal and year-to-year water availability (International Energy Agency, 2021b). The impacts of droughts can extend beyond hydroelectric facilities, as they can reduce the efficiency of thermal power plants that rely on water for cooling processes, creating complex system-wide vulnerabilities that can propagate through interconnected electricity markets. These compounding effects raise critical questions about how electricity systems adapt to water stress in both the short and long term, with implications for energy security, environmental outcomes, and climate resilience.

The effects of climate change—particularly droughts—on electricity systems vary substantially across regions, shaped by electricity matrix composition, exposure to climate risks, infrastructure characteristics, and institutional settings (International Energy Agency, 2021b; Yalew et al., 2020). While a growing literature examines the effects of drought on electricity systems using observational data (Eyer and Wichman, 2018; Qiu et al., 2023; An and Zhang, 2023b), the evidence remains relatively limited and focused mostly on developed regions such as the United States and Europe, as well as China. This knowledge gap is particularly critical for a region such as Latin America and the Caribbean, where hydropower accounts for more than 45% of electricity generation—a figure substantially above the global average. This dependence gives rise to vulnerabilities to climate-induced hydrological changes (International Energy Agency, 2021a; Bagnoli and Cavallo, 2025). The region faces potentially distinct adaptation challenges: its high reliance on hydropower may amplify its vulnerability to droughts, while its transmission infrastructure and market structures may constrain compensatory responses on the part of other generation technologies. An understanding of these dynamics is essential not only for adapting to climate risk in these regions but also for anticipating how electricity systems globally might respond to increased water stress under climate change scenarios.

In this paper, we examine the effects of droughts on electricity generation from 2000

to 2024 in Chile, which stands out for several reasons as a compelling context in which to examine and better understand how electricity systems adapt to water stress. First, hydropower plays a critical role in the country's electricity generation, accounting for 36% of electricity production during our sample period, which makes the sector particularly vulnerable to prolonged periods of water scarcity. This vulnerability has been acute during recent decades as a megadrought (*megasequía*) has affected the river basins between the Coquimbo and Araucanía regions, the location of the vast majority of the country's hydroelectric generation (Center for Climate and Resilience Research, 2021). Second, Chile's distinctive geography, with its parallel river basins flowing from the Andes to the Pacific Ocean, creates natural variation in drought exposure across basins within the same electricity market. This spatial configuration allows us to examine how different generation technologies respond to drought conditions and distinguish between local (basin level) and system-wide (national) drought effects while national institutional settings remain constant across regions. Additionally, this regional variation, combined with the availability of plant-level data spanning 25 years, allows us to analyze adaptation patterns across different time scales—from immediate operational responses to longer-term investment decisions.

Taking advantage of this ideal setting, we examine how drought conditions affect electricity generation across technologies over time. Our empirical approach integrates plant-level generation records, detailed meteorological data, and basin-level measures of drought incidence to analyze relationships between water scarcity and electricity production patterns. We leverage variation in drought exposure across 46 river basins from 2000 to 2024, controlling for plant characteristics and local weather conditions. This approach allows us to compare electricity generation across plants experiencing different drought conditions during the same period while we account for plant-specific factors and market-wide temporal shocks.

Before examining the impacts of droughts, we characterize the evolution of Chile's electricity generation portfolio over 2000–2024. We document profound transformations marked by substantial growth in thermal capacity since 2000 and increasing market atomization—defined as decreasing average generation per plant over time—from 2010. This trend occurred across both thermal and hydropower generation technologies, with a rising number of smaller electricity plants entering the market. Hydropower generation shifted predominantly toward smaller-scale run-of-river and small hydro installations because of heightened environmental regulations and weather variations. The market structure was further transformed by the rapid development and integration of solar photovoltaic and wind energy projects after 2014. These changes collectively reshaped the country's generation mix and potentially altered its vulnerability to climate impacts.

Our analysis of drought effects reveals several key findings with important implications for electricity system adaptation. First, we find that local droughts significantly reduce hydroelectric generation by approximately 24.5%. Second, we document complex system-wide response dynamics, with thermal plants that have above-median available capacity increasing generation by approximately 28% during drought episodes in their own basins. Additionally, the plants with available capacity also increase generation by 36.9% in response to national drought conditions. This dual response to both local and national drought conditions suggests that market integration only partially mitigates drought shocks. This partial mitigation implies that the impacts of drought are spatially concentrated, with drought-affected regions facing both direct water scarcity effects and increased local air pollution from compensating thermal generation. Third, we quantify the environmental costs of this thermal substitution. Emissions from high-capacity thermal plants rise by roughly 34% during system-wide droughts, translating to an estimated 1.09 $MtCO_2$ per year over our sample period. This increment represents approximately 1.4–1.8% of Chile's annual national emissions and 5.5–6.5% of the power sector's total CO_2 emissions, underscoring how drought-induced adaptation creates a direct climate feedback loop. Fourth, examining investment patterns, we find that prolonged droughts are followed by increases in both thermal and wind capacity, with solar showing positive but more delayed adjustments; hydropower exhibits no systematic response. These patterns indicate that sustained hydrological stress reshapes long-run investment portfolios, promoting diversification into wind and solar while also increasing thermal capacity, raising concerns about long-term carbon lock-in.

Our study makes three distinct contributions to the literature. First, we advance research on the short-run impacts of drought on electricity generation (Eyer and Wichman, 2018; Herrera-Estrada et al., 2018; An and Zhang, 2023b,a). Most empirical evidence on technology substitution during drought comes from the United States, Europe, and China, and studies for Latin America and the Caribbean remain limited despite the region's heavy reliance on hydropower. Existing work for the region is largely aggregate or simulation-based (del Mar Rubio and Tafunell, 2014; International Energy Agency, 2021a; González-Lorente et al., 2024; Hunt et al., 2018), with only recent plant-level evidence focusing primarily on emissions rather than generation or capacity investments (Eriksson et al., 2025). Our analysis extends this literature by providing plant-level evidence on system-wide adaptation, showing that thermal compensation depends critically on plants' available capacity and that thermal units respond to both local and national drought conditions—an interaction margin not previously documented in hydropower-dependent systems.

Second, we connect short-run operational responses to long-run investment dynamics

(Elliott, 2022; Ömer Karaduman, 2021) by showing how prolonged hydrological stress affects capacity expansion. Existing work on investment under climate stress relies largely on model-based simulations (Cohen et al., 2014; Ralston Fonseca et al., 2021), and empirical evidence remains limited. We document that multiyear droughts are followed by increases in thermal capacity and, more gradually, in wind and solar, with no systematic adjustment in hydropower. These responses generate a climate feedback: drought-induced water scarcity accelerates carbon-intensive expansion even as it promotes some diversification. While Harris (2024) studies drought-driven technological choices among thermal plants in Texas, we provide multi-technology evidence in a hydro-dependent system where water scarcity is central to energy security.

Third, we situate our analysis within the broader evolution of electricity markets in Latin America (del Mar Rubio and Tafunell, 2014)—and in Chile in particular (Gaete-Morales et al., 2018; Bauer, 2009; Serra, 2022; Vega-Coloma and Zaror, 2018)—where most work has examined regulatory and environmental aspects. Much less attention has been given to the sector's structural transition toward a more fragmented set of smaller and more numerous generation units. This finding, which emerges naturally from our entry analysis, provides context for our main results: responses to prolonged drought occur in a system that has become more diversified across technologies and scales, shaping how hydrological stress affects investment and generation decisions.

Our findings have significant implications for energy policy, climate adaptation, and emissions trajectories. The identified patterns of drought vulnerability and thermal compensation highlight a critical tension in electricity systems. Adaptations that maintain short-term reliability may undermine longer-term climate sustainability. When drought reduces hydroelectric output, the resulting shift toward thermal generation increases emissions precisely when the affected regions already face water scarcity. Moreover, our finding that drought historically correlated with thermal capacity investment suggests that climate-induced water stress could create path dependencies that lock in carbon-intensive infrastructure. This self-reinforcing cycle—whereby climate impacts trigger adaptations that exacerbate climate change—poses significant challenges for decarbonization efforts in regions with high hydropower dependence. Our results underscore the importance of incorporating climate resilience into electricity system planning and suggest that policies promoting drought-resistant, low-carbon technologies may yield substantial co-benefits for both adaptation and mitigation. As climate change intensifies drought frequency and severity in many regions, an understanding of these complex dynamics is increasingly urgent to inform the design of resilient, sustainable electricity systems.

The remainder of this paper is organized as follows. Section 2 provides background on Chile's electricity sector and presents stylized facts about its transformation over time.

Section 3 describes our dataset combining plant-level generation, meteorological data, and drought measures. Section 4 presents our analysis of the effects of drought on electricity generation across technologies, thermal plant responses, and investment patterns. Section 5 discusses policy implications and concludes.

2 Chile's Electricity Generation System

Historically, Latin American and the Caribbean electricity markets have been dominated by hydropower, given the region's abundant hydrologic resources. Chile exemplifies both this traditional dependence and the challenges it creates in a changing climate. The country's electricity sector has undergone significant transformations over recent decades—from a system once heavily reliant on large hydropower reservoirs to one boasting a diversified generation mix today.

2.1 Institutional framework

In 1982, Chile's electricity sector underwent a radical transformation, with its vertically integrated structure unbundled into generation, transmission, and distribution functions.[1] This reform laid the groundwork for the emergence of two distinct generation markets: the Sistema Interconectado Central (SIC) and the Sistema Interconectado del Norte Grande (SING). The SIC, established in 1982 with its own system operator, capitalized on the country's abundant hydroelectric resources in the central regions. In contrast, the SING, created in 1993 with its own dedicated system operator, developed in the northern regions characterized by relative water scarcity.

The evolution of the sector continued with significant reforms in 2017 that further integrated these previously separate systems. Advances in infrastructure and regulatory oversight converged to facilitate the physical interconnection of the SIC (which historically contributed about 73.5% of total generation) and SING (which provided approximately 25.8%). The construction of a 500 kV transmission line between Cardones and Polpaico established the essential physical link, a connection reinforced in November 2017 with the commissioning of a double-circuit transmission line. Simultaneously, under Law 20.936 of 2016, regulatory reforms led to the creation of El Sistema Eléctrico Nacional (SEN) and the establishment of a new independent system operator (ISO) to succeed the former joint operator of the SIC and SING.[2] Today, this unified system serves more than 99.3%

[1] This subsection draws from Serra (2022) unless otherwise noted.

[2] In addition to the ISO, two regulatory bodies oversee the sector: the National Energy Commission

of the country, with only 0.7% of the population relying on isolated systems.

Market concentration at the company level was very high throughout the 1990s and 2000s, only beginning to decline in more recent years. In 1990, the three largest generators produced nearly 97% of SIC generation, and their combined share remained about 95% in 1995 and above 90% through 2010. Concentration started to fall more visibly in the second half of the 2010s, dropping to roughly 78% in 2015 and 75% in 2017, reflecting the gradual entry of a larger number of smaller generation companies (Serra, 2022).

In the early 1990s, the electricity market was dominated by large-scale hydroelectric dams and coal-fired power plants. However, beginning in the early 2000s, significant structural changes emerged, driven by factors such as free entry in the generation sector, the implementation of cost-based markets designed to inhibit market power, growing environmental concerns, increasing public opposition to large infrastructure projects, and favorable economic conditions for renewable energy adoption (Serra, 2022; Pollitt, 2004). Specifically, declining costs and the substantial potential associated with solar and wind technologies accelerated the proliferation of smaller-scale renewable energy projects, reshaping the competitive landscape of the electricity sector.

The sector experienced substantial regulatory transformation between 2000 and 2024, a period marked by strategic reforms aimed at reducing entry barriers and fostering growth in variable renewable energy (VRE). The initial reforms targeted structural inefficiencies in transmission pricing, which had previously hindered investment. Law 19,940 (2004) significantly redefined the sector by classifying transmission as a public service, instituting mandatory transmission expansion planning, restricting ownership concentration, and clearly delineating cost allocation mechanisms. Additionally, a set of reforms in 2005 introduced international competitive auctions with longer-term contracts and indexed pricing, substantially improving market predictability and stability.

Subsequent legislation further promoted the installation of small renewable energy capacity. Decree with Force of Law (DFL) No. 4 (2007) established guaranteed grid access for small-scale distributed generation projects of up to 9 MW, implementing a graduated exemption framework for transmission costs. Law 20,257 (2008), Chile's renewable portfolio standard, mandated progressively increasing targets for renewable energy sourcing, significantly accelerating development of nonconventional renewable energy. This standard was further strengthened by Law 20,698 (2013), which stipulated a rise in the renewable sourcing requirement to 20% by 2025 and introduced biannual compliance auctions to ensure achievement of targets.

(CNE), which develops technical regulations and calculates regulated tariffs, and the Ministry of Energy, which sets broader sectoral policies.

The integration of Chile's northern (SING) and central (SIC) electricity grids into the unified SEN in 2017 was a crucial milestone. This integration facilitated efficient inter-regional electricity trading, considerably boosting market competitiveness for renewable sources and incentivizing further renewable energy investment (Gonzales et al., 2023).

2.2 Geography, Climate and Drought Context

Chile's distinctive geography shapes its energy landscape. Spanning from the arid Atacama Desert to the Mediterranean-like central valleys and cooler southern regions, the country's diverse climatic zones create varied water resources through river basins flowing from the Andes to the Pacific. As shown in Figure 1, this geographical diversity directly influences electricity infrastructure in the SEN. The arid north hosts energy-intensive mining operations served primarily by thermal and solar installations, while the water-rich central region supports hydropower generation. Wind farms occupy strategic coastal positions. Despite their greater number, solar installations have smaller individual capacities than hydropower and thermal plants.

Figure 2 provides, as an example, a detailed view of the Bio Bio basin's generation technologies. Its hydropower infrastructure includes large reservoir plants (blue dots with construction years: 1973, 1981, 1996, 2004, and 2014) and smaller run-of-river plants. Generation capacity is reflected in dot size across all plant types: thermal (red), wind (green), and solar (orange). The visualization reveals clear spatial organization: reservoir plants in the Andean foothills, run-of-river plants along rivers, thermal plants near coastal urban areas, wind farms on coastal sites, and solar installations throughout.

Chile has faced significant hydrological challenges affecting electricity supply. A 1998 drought coinciding with La Niña (a Pacific Ocean cooling pattern bringing drier conditions to Chile) exposed vulnerabilities, leaving 500 GWh of demand unmet and reducing inflows at the Laja reservoir by 65% (Fischer and Galetovic, 2003; Bauer, 2009; Pollitt, 2004). More recently, an unprecedented megadrought (2010–2020) affected the river basins between Coquimbo and Araucanía hosting most of the country's hydropower generation (Center for Climate and Resilience Research, 2021), which created complex adaptation challenges for both operations and planning. Climate change projections indicating increasing drought severity, combined with rising electricity demand, stricter environmental regulations, and declining costs of alternatives, have transformed Chile's generation portfolio. Understanding these hydrological patterns remains crucial for future electricity system planning.

2.3 Evolution of Generation Portfolio

Chile's electricity generation portfolio has transformed substantially over time, balancing traditional hydropower generation with thermal generation while incorporating growing shares of solar and wind technologies. This evolution reflects responses to resource constraints, policy changes, and technological advancements, creating distinct patterns across regions and time.

Chile's electricity generation underwent dramatic shifts between 2000 and 2024, driven by interrelated factors of resource constraints, policy decisions, and economic considerations. Figure 3 reveals how the initially balanced mix of thermal and hydropower sources shifted significantly around 2010, coinciding with the onset of the megadrought. As water availability declined in hydropower-rich central regions, thermal generation increased substantially to compensate, demonstrating the system's structural response to this resource constraint. By 2013, thermal generation was double that of hydropower.

This shift toward thermal generation occurred despite Chile's limited domestic fossil fuel resources, reflecting a strategic response to the hydropower vulnerabilities exposed by the drought events discussed above. The expansion of thermal power capacity was driven by both the need for supply reliability and rapidly growing electricity demand, with coal emerging as the economically preferred option due to its comparatively lower levelized cost of energy (Serra, 2022). The sudden disruption of Argentine natural gas imports in 2006 further accelerated this trend, forcing Chile to increase coal dependency while converting natural gas plants to diesel operation. The subsequent development of liquefied natural gas (LNG) infrastructure later enabled natural gas reintegration into Chile's energy matrix (Vega-Coloma and Zaror, 2018).

Since 2018, coal-fired electricity generation has faced increased public opposition resulting in policy commitments to phase coal out by 2040. This policy shift, formalized in a 2019 stakeholder agreement, prompted accelerated retirements and conversions of coal plants (Moreno et al., 2024). Panel (b) of Figure 3 shows the evolution in plant numbers by technology type. Between 2009 and 2013, thermal plants expanded rapidly, accompanied by increased thermal generation. After 2013, the number of thermal plants stabilized, whereas the number of hydropower plants grew gradually. Renewable energy sources, particularly solar, grew exponentially from 2013 onward, though these facilities generally featured lower installed capacity per plant.

The 2017 integration of separate systems, coupled with declining technological costs, boosted investments in solar and wind capacity, particularly in the solar-rich Atacama Desert. This enabled efficiency gains through electricity trade between regions (Gonzales

et al., 2023). Figure 4 illustrates how geographical differences shaped generation patterns in the former SIC and SING regions. Given their distinct resource endowments, the systems evolved differently: The SIC's thermal generation increased markedly after 2010, likely compensating for declining hydropower during the megasequía, while the SING maintained relatively stable thermal output largely serving mining operations. Nonconventional renewable adoption also followed different trajectories in the two systems: The SING saw earlier and more extensive solar penetration, capitalizing on the Atacama's abundant resources, while the SIC developed a more balanced mix of wind and solar, with wind farms leveraging the coastal conditions in Chile's central-southern zone.

The hydropower sector underwent a fundamental transformation in response to hydrological vulnerabilities. Despite these challenges, the sector maintained its relevance through a structural shift toward smaller installations. Table 1 quantifies this shift: Of the 164 hydropower plants in the sample, only 11 (6.71%) are reservoir plants, with just 3 new reservoir plants added after 2000. The vast majority of the expansion corresponded to nonreservoir plants (including run-of-river and mini-hydro plants), which comprise 129 of the 132 plants (78.66% of the total) added after 2000. This massive entry of smaller nonreservoir plants effectively sustained the hydropower sector even as older plants struggled with drought conditions.

Figure 5 illustrates the contrasting trajectories between established and new hydropower plants. Panel (a) depicts the generation from plants already active before 2000, showing how established plants faced challenges during the drought period. Pre-2000 reservoir plants experienced a decline from peak production of about 15,000 GWh in 2005 to approximately 6,000 GWh by 2020, with some recovery by 2025. Similarly, older run-of-river plants declined more gradually from around 7,000 GWh to 3,500 GWh. Panel (b) shows the generation from plants added after 2000, revealing growth in run-of-river generation from near zero to approximately 6,000 GWh by 2025. New reservoir plants, though fewer in number, contributed significant but more volatile generation, with peaks around 5,000 GWh. The contrasting trends between the two panels suggest that the hydropower sector was sustained by the entry of numerous smaller plants even as established plants declined. The expansion of primarily run-of-river installations helped offset some of the production losses from established plants. This transformation represents a strategic response by Chile to both climate uncertainty and environmental policy shifts, resulting in a hydropower system increasingly characterized by numerous smaller, distributed generation assets rather than dominated by a few large reservoir facilities.

3 Data

To evaluate the impact of droughts on electricity generation, we exploit variation in exposure to hydrological droughts among all power plants connected to Chile's main grid (the SEN). We characterize droughts at the basin level using watershed boundaries and monthly runoff data, with plants' exposure determined by their geographical location in these basins. Our dataset combines monthly generation records and detailed plant characteristics with hydrological conditions and a set of climatic controls for 2000–2024.

3.1 Power Plant Data

Our primary source of generation data is the National Electricity Coordinator (Coordinador Eléctrico Nacional, 2024), whose data structure reflects the evolution of Chile's electrical systems over time. From 2000 to 2015, generation data were recorded separately for the SING at daily frequency and the SIC at hourly frequency. Since 2016, under the unified SEN, the data have been recorded hourly.

Table 2 presents summary statistics of our power plant data. Panel (a) shows aggregate statistics for all plants, including their net-effective capacity at the end of the period[3], market participation in SIC or SING as of 2000, activity status in 2000, commissioning year, and number of generation units. The subsequent panels break down these statistics by technology type of generation technology: thermal (Panel (b)), hydroelectric (Panel (c)), wind (Panel (d)), geothermal (Panel (e)), and solar (Panel (f)).

3.2 Climate Data

Climate data comes from the International Energy Agency's (IEA's) Weather, Climate and Energy Tracker (International Energy Agency, 2024a), which provides high-resolution weather-related data relevant for analyzing energy systems. While the dataset offers a comprehensive range of variables, we focus on key controls: mean air temperature (at 2 meters above surface level, in Celsius), wind speed (10 meters above surface level, in meters per second), relative humidity (based on 2-meter air and dew temperatures, in percentage), precipitation (in millimeters per hour), and surface atmospheric pressure (in pascals [Pa]). These variables are available monthly from 1979 onward on a fine-resolution grid of 0.25 degrees.[4]

[3]Reported by the system operator; available for the final period in our data. Accessed in January 2025.

[4]See International Energy Agency (2024b) for detailed documentation of the dataset.

For our analysis, we use climate data corresponding to our study period of 2000–2024. To obtain plant-specific measures of local weather conditions, we calculate zonal statistics for each climate variable within a 10-kilometer buffer around each power plant's location.

3.3 Drought Measurement

To capture water availability, we construct monthly basin-level measures of hydrological droughts for the 2000–2024 period. Runoff, representing water flowing both over land surfaces and through subsurface layers, serves as a key indicator of water availability. The IEA dataset measures runoff in mm/h, representing the depth of water that would accumulate if spread evenly over a grid box area (International Energy Agency, 2024b). Following previous literature on hydroclimatic impacts on energy systems (Herrera-Estrada et al., 2018; Eriksson et al., 2025; Qiu et al., 2023), we quantify drought conditions using runoff anomalies—periods where water availability deviates from normal levels. This approach has the advantage of allowing us to account for seasonal variations by comparing water availability with its typical levels in the respective calendar-month, which ensures that water scarcity is flagged only when runoff deviates from its expected seasonal norm.

For each pixel in each month, we calculate monthly runoff anomalies by comparing the current runoff to long-term calendar–month averages over the entire historical period.[5] To capture the persistent nature of drought, instead of short-term variations in water availability, we then compute cumulative anomalies over different windows (from 3 to 12 months).

To quantify these anomalies, we need to specify a geographic area in which to define the presence of drought. To do so, we integrate runoff estimates from the IEA's Weather, Climate and Energy Tracker (International Energy Agency, 2024a) with watershed boundaries from the HydroBASINS database (Lehner and Grill, 2013). We aggregate the cumulative anomalies at the level-06 as defined in HydroBASINS and obtain a binary measure of drought that indicates whether the average cumulative runoff anomalies are below -1 times the standard deviation of the historical distribution for that basin. Overall, this approach allows us to identify periods of abnormally low water availability across diverse hydrological basins for each month. Annex A.3 presents the details of the process.

Overall, Chile comprises 46 HydroBASINS Level-06 units with power plants, exhibiting substantial temporal and spatial variation in drought exposure. Figure 6 shows the

[5]The IEA dataset provides global coverage at a detailed spatial resolution with temporal coverage extending from 1979 to the present.

evolution of drought conditions over 2000–2024. The simple (unweighted) average of local droughts, shown in red, displays increasing frequency over time but also marked fluctuations—for instance, no basin is in drought between 2018 and mid-2020. The weighted national drought index, shown in blue and constructed using hydro-capacity weights[6], exhibits much sharper movements during major drought episodes (2007–2008, 2010–2011, 2016–2017, and 2020–2022), reflecting the disproportionate influence of hydro-relevant basins on systemwide drought conditions. Figure 7 complements this temporal evidence by showing the geographic distribution of drought exposure. Droughts occur throughout the country but are more frequent in the south, where the most affected basin is in drought about 26% of the months in our sample (2005–2024). This temporal and spatial variability is central to our empirical strategy.

4 Effects of Droughts on Electricity Generation

In this section, we investigate how drought conditions affect electricity generation across different technologies and over time. We begin by detailing our empirical approach in Section 4.1. We then quantify the differential impacts of drought on generation across technologies (Section 4.2), finding substantial reductions for hydropower plants but no significant impacts for plants using other technologies. We then explore thermal plants' responses in greater detail (Section 4.3), examining how their behavior varies with spare capacity and in response to both local and system-wide droughts. We quantify the environmental implications of thermal substitution in Section 4.4, translating the generation responses into emissions changes and assessing their magnitude relative to national and sectoral CO_2 totals. Finally, we investigate how drought influences investment in new generation capacity (Section 4.5), with implications for long-term emissions trajectories and stranded asset risks. Throughout our analysis, we employ various robustness checks and specifications to ensure the reliability of our findings and better understand the mechanisms through which droughts affect electricity systems.

4.1 Empirical Approach

We estimate the impacts of drought on electricity generation with the following fixed effects regression:

$$\text{Generation}_{ibmt} = \beta drought_{bt} + \mathbf{X}_{it}\gamma + \alpha_i + \alpha_{tm} + \varepsilon_{ibmt} \tag{1}$$

[6]See sub-section 4.3.2 for the definition of the hydro-capacity weights underlying the national drought index.

where Generation_{ibmt} is the average daily electricity generation (in MWh) of plant i located in basin b of market m during time t.[7] The subscript t indexes month–year combinations, while m denotes the electricity market where the plant operates.[8] The variable $drought_{bt}$ is our binary drought indicator for basin b at time t, constructed as described in Section 3.3. The coefficient of interest β represents the causal impact of drought on electricity generation.

Following Eriksson et al. (2025), we include in the vector $\mathbf{X}_{it}$ time-varying meteorological controls for the area within a 10-kilometer radius around each plant. These controls include mean air temperature (at 2 meters above surface level, in Celsius), wind speed (10 meters above surface level, in meters per second), relative humidity (based on 2-meter air and dew temperatures, in percentage), and precipitation (in millimeters per hour). We also include plant fixed effects α_i to control for time-invariant plant characteristics, such as capacity and technology type. Since plants do not change basin over time, these fixed effects also capture any basin-level time-invariant characteristics. Additionally, we include market-specific time fixed effects α_{tm} to absorb any temporal shocks common to all plants within each electricity market, such as seasonal patterns or macroeconomic fluctuations. Importantly, these time fixed effects account for demand shocks that affect electricity generation.

Our analysis employs balanced panels of plants to isolate the effect of drought on generation from any effects related to entry. For hydropower and thermal plants, our main analysis includes only plants that began operation before 2005, while for solar and wind technologies, we include plants that were operating before 2015 because of their later deployment in the market.

The main identifying assumption of this model is that drought is a medium-term weather trend and hence that its effect on electricity generation can be differentiated from the effects of weather patterns and seasonal demand shocks. As a result, conditional on our accounting for seasonal trends, temperature, and other demand shocks, the effect of variation in water scarcity on electricity generation is a plausibly exogenous shock to electricity supply. Thus, the identification of β relies on our comparing generation across plants that experience different drought conditions during the same period and market, with controls for plant-specific characteristics and local weather conditions. This approach assumes that, conditional on the inclusion of controls and fixed effects,

[7] We calculate daily generation by dividing monthly generation totals by the number of days in each month, ensuring comparability across months of different lengths.

[8] For years before the 2017 integration, m refers to either the SIC or SING market. For the years after their unification into the SEN, m represents the integrated national market. This distinction is important for our market-specific time fixed effects, which are separate for SIC and SING for the years before their integration and common afterward. See Section 2 for further details.

drought occurrence is as good as random. More specifically, we assume there are no time-varying confounders at the basin level that simultaneously affect drought conditions and electricity generation through channels other than our measured drought indicator. This empirical design allows us to quantify the degree of vulnerability to drought across different generation technologies, providing insights into how electricity systems may respond to increasing climate variability in the future.

4.2 Drought Vulnerability Across Generation Technologies

4.2.1 Main Results

We begin by examining how drought affects electricity generation across different technologies. Following our empirical strategy outlined in Section 4.1, we estimate Equation 1, which includes plant fixed effects to control for time-invariant unobservables and market–time fixed effects to account for market-wide demand and other temporal shocks. We progressively introduce meteorological controls to isolate the effect of droughts from the effects of other weather-related factors. Throughout our analysis, we present results from our preferred specification with full meteorological controls (column 7 in Tables 3–7).

Table 3 shows the impact of drought on electricity generation for all plants. The coefficient on drought is negative and statistically significant across all specifications, ranging from -0.149 in the baseline with only fixed effects (column 1) to -0.154 in the specification with full controls. This indicates that, overall, drought reduces electricity generation by 15.4% in the affected river basins, which highlights the substantial system-wide impact of drought conditions.

Different generation technologies, however, show markedly different responses to drought conditions. Hydropower plants, which directly depend on water availability, exhibit the strongest negative response. As shown in Table 4, the drought coefficient for hydroelectric plants is negative and significant at the 1% level across all specifications, ranging from -0.233 in the baseline model to -0.245 in that with full controls. This translates to a 24.5% reduction in electricity generation for hydropower plants in drought-affected basins in comparison to the generation of those in nondrought basins—a substantial decrease that underscores the vulnerability of hydropower to changing water availability.

Thermal plants, by contrast, show a different pattern. According to Table 5, the drought coefficient is positive but small and statistically insignificant across all specifications, varying between 0.013 and 0.023. This shows that the electricity generation from thermal plants does not respond to local droughts. This average effect, however, masks

important heterogeneity in thermal plant responses that we explore in Section 4.3.

For renewable technologies that do not directly depend on water availability, we find no statistically significant impact of drought on electricity generation after we control for relevant climatic factors. For solar generation, the drought coefficient remains negative across all model specifications (ranging from -0.042 in the baseline to -0.039 in the model with full controls) but never reaches statistical significance, as shown in Table 6. Similarly, wind generation shows no significant relationship with drought conditions, with coefficients that vary from -0.038 in the baseline to 0.026 in the model with full controls but that remain statistically insignificant throughout (Table 7). These findings align with the fundamental characteristics of these technologies–both are nondispatchable, with near-zero marginal costs, generating electricity whenever their primary energy source (sunlight or wind) is available, regardless of drought conditions. During our period of analysis, large-scale energy storage technologies remained prohibitively expensive and largely unavailable at commercial scale, meaning there was limited ability to shift generation from these renewable sources in response to system needs.

Figure 8 summarizes these results visually, plotting the drought coefficients from our preferred specification for different technology types across different samples. Panel (a) shows results for hydroelectric and thermal plants for the period 2005–2024. Panel (b) presents results for all technology types (including solar and wind) for the shorter period 2015–2024, when there were more solar and wind plants in operation. Panels (c) and (d) restrict the sample to the SIC market for the same technology groupings and time periods as in Panels (a) and (b), respectively.

Across all the panels, we consistently observe significant negative effects on hydropower generation (approximately -24% to -28%), while the response of thermal, wind, and solar plants is not statistically different from zero. The overall effect on generation (labeled "All") is consistently negative and significant, ranging from -11% to -15%, depending on the sample.

To assess the robustness of our main findings, we next explore whether the estimated effects of drought vary across plant cohorts, time periods, and specifications. These analyses not only validate our baseline results but also provide additional insights into temporal patterns of drought vulnerability in the electricity sector.

Moreover, the main findings establish that drought conditions create a significant shift in the generation mix by substantially reducing hydropower output. For other technologies, the mere fact that a plant is located in a drought-affected basin does not significantly affect its electricity generation. However, when drought reduces hydropower

generation in these basins, the overall response in generation may occur elsewhere, as other technologies are not affected by the local drought conditions. This broader response would not be captured by our previous specification focused solely on the local effects of drought. We will investigate this possibility after the heterogeneity and robustness analyses to clarify which mechanisms drive the response of the electricity system to reduced hydropower generation caused by local droughts.

4.2.2 Heterogeneity and Robustness Analyses

We extend our analysis to examine three important dimensions that might influence our main findings: whether the estimated drought effects are sensitive to the composition of plants in our sample, whether these effects vary over time because of changing climatic conditions, and whether our results are robust to alternative definitions of drought incidence. These analyses serve both as robustness checks and as explorations of potential effect heterogeneity.

In Figure 9, Panels (a) and (b), we show estimates from our test of robustness to sample selection, where we fix the period of analysis (2015–2024) but vary the plant cohorts included. Each point estimate represents the drought effect for plants that began operation in or before the year indicated on the x-axis. For example, the coefficient labeled "2006" represents the drought effect for plants that started operation in 2006 or earlier. This approach helps us assess whether our main findings are driven by specific cohorts of plants or are consistent across different generations of electricity infrastructure.

For hydropower plants (Figure 9, Panel (a)), we find a remarkably consistent negative effect of drought on generation across all cohort specifications, with point estimates consistently around -0.30 to -0.35. This consistency across cohorts indicates that the vulnerability of hydropower generation to drought conditions is an inherent characteristic of power generation with this technology, not specific to older or newer installations. For thermal plants (Figure 9, Panel (c)), we observe that the drought coefficient remains relatively stable across the different cohort specifications, hovering around zero with slightly positive point estimates. This suggests that the limited average response of thermal plants to local drought conditions is consistent across different generations of plants.

In Figure 9, Panels (b) and (d), we present the results from a rolling-window analysis in which we examine temporal variation in drought effects. We restrict the sample to plants that began operation before 2005 and analyze the effects across time periods to isolate how drought impacts have evolved over time, independently of changes in the plant mix. Each point estimate represents the effect of drought for a 5-year period, with the year

label indicating the midpoint of the window. For example, the coefficient labeled "2007" represents the drought effect for the period 2005–2009, while "2012" covers 2010–2014, and so on through 2022 (which covers 2020–2024).

The rolling-window analysis for hydropower plants (Figure 9, Panel (b)) reveals an interesting temporal pattern: The magnitude of the negative effect temporarily decreases for the windows centered on 2009–2013 before intensifying significantly for the windows centered on 2014 and beyond. This pattern aligns with documented drought cycles in the region, with particularly severe droughts occurring in the latter periods. The increasingly negative coefficients for later windows (centered on 2016–2022) suggest that the impacts of droughts on hydroelectric generation have become more pronounced over time, possibly because of severer drought conditions in recent years. For thermal plants (Figure 9, Panel (d)), the rolling-window analysis confirms that thermal plants' reaction to local droughts remained mostly insignificant throughout the period, with the effects becoming slightly negative and significant only around the periods centered on 2012 and 2013.

To ensure the robustness of our findings to different definitions of drought, we conduct extensive sensitivity analyses by varying both the spatial extent and temporal accumulation of our drought measure. While Figure 8 presents results from our baseline specification (12-month accumulation, level 06 basin), Appendix Figures A1 and A2 demonstrate the robustness of our results to our using different spatial aggregations (basin levels 04 through 08), while Appendix Figures A3 and A4 show results for droughts defined on the basis of different temporal accumulation periods (from 3 to 36 months). The effects of droughts on hydropower generation are consistently negative across all specifications. Thermal generation shows a statistically insignificant effect in most cases. The consistency of these patterns across twenty-five different specifications—covering five spatial levels and five temporal accumulation periods—reinforces the reliability of our main findings regarding hydropower vulnerability to droughts and the lack of a significant response of thermal generation to local droughts conditions.

Finally, to account for extreme values and observations with zero generation in our sample, we compare the results from two estimation approaches in Table 8. While conventional ordinary least square (OLS) with log-transformed dependent variables (results on odd-numbered columns) provides a straightforward interpretation of elasticities, it cannot accommodate zeros. This limitation is particularly relevant for thermal generators, which, in contrast to hydro plants, may experience temporary shutdowns or permanent exits from the market. Poisson Pseudo-Maximum Likelihood estimation (PPML; results in even-numbered columns) addresses these challenges by directly modeling the conditional mean without requiring log transformation. The similarity of the results across both methods reinforces the robustness of our findings.

These analyses provide important context for the interpretation of our main results. That we consistently find a negative impact on hydropower generation across different cohorts, time periods, drought definitions, and estimation methods reinforces our conclusion that droughts significantly constrain hydropower output. The temporal intensification of drought impacts raises concerns about the resilience of electricity systems to future drought conditions, especially as climate change is projected to increase the frequency and severity of droughts in many regions.

4.3 Thermal Plants' Response to Drought

While our analysis thus far has established the robust negative impact of drought on hydroelectric generation and the limited average response from thermal plants, these findings mask potentially important heterogeneity in thermal plants' behavior. In this section, we delve deeper into these dynamics by examining how thermal plants' responses vary with the plants' spare capacity and whether they respond differently to local and national drought conditions.

First, the average effect may mask heterogeneous responses to droughts by thermal plants. Some plants may face effective capacity *derating* when cooling-water is constrained or intake-water temperature rise, which reduces efficiency and the effective capacity of the plant (Van Vliet et al., 2016). On the other hand, other plants may expand their generation if they have spare capacity to meet hydropower shortfalls. Hence, the first question that we aim to answer in this subsection is whether thermal plants can increase their output when hydropower generation declines, and whether these effects depend on their available spare capacity.

Second, while droughts are local, in an integrated electricity system, a thermal plant could adjust its output to address hydroelectric shortages regardless of its location. Therefore, in a perfectly integrated market, local drought conditions do not directly affect local thermal generation; instead, plants would respond to national drought conditions whenever needed. However, when transmission constraints are present, markets can become segmented, and thermal plants may respond primarily to local conditions. This spatial dimension is particularly important for the environmental externalities of drought responses, as increased thermal generation in drought-affected regions can concentrate air pollution and other emissions in already vulnerable areas. To understand these dynamics, the second question this subsection aims to answer is whether thermal plants adjustments remain local or spread across regions through market integration.

4.3.1 Spare Capacity

To measure spare capacity, we construct an indicator of unused generation potential based on each plant's historical performance.[9] This measure captures how much additional electricity each plant could potentially generate beyond its typical operation levels. Specifically, for each plant and month, we calculate the difference between its maximum and average daily generation over the last 12 months:

$$\widehat{capacity}_{it} = g_{it}^{max} - g_{it}^{avg}$$

$$g_{it}^{max} = \max_{s \in [t-12, t-1]} g_{is}$$

$$g_{it}^{avg} = \frac{1}{12} \sum_{s \in [t-12, t-1]} g_{is}$$

where g_{it}^{max} is the maximum daily generation of plant i in the last 12 months and g_{it}^{avg} is the average daily generation over the same period. This measure represents the additional generation potential that each plant has demonstrated in the recent past rather than its total installed capacity. We then create a binary indicator for plants with high spare capacity according to whether their unused generation potential is above or below the sample median. This allows us to examine whether plants with relatively more room to increase generation within their local market are more responsive to drought conditions.

To analyze the differential response of plants with high and low spare capacity to drought conditions, we extend our baseline specification:

$$\begin{aligned} \text{Generation}_{ibmt} = \beta_1 \text{Drought}_{bt} + \beta_2 \text{Spare}_{ibt} + \beta_3 (\text{Drought}_{bt} \times \text{Spare}_{ibt}) \\ + \mathbf{X}_{it}\gamma + \alpha_i + \alpha_{tm} + \varepsilon_{ibmt} \end{aligned} \tag{2}$$

where Spare_{ibt} is an indicator equal to one if plant i's spare capacity (unused generation potential) is above the national median at time t. The coefficient β_3 captures how responses to drought conditions vary between plants with high and low spare capacity.

Table 9 presents our estimation results using the capacity measures based on the

[9] We observe a single reported value of net effective capacity from the system operator at the end of the sample period. Although one could compare observed generation to this figure, doing so would implicitly assume that capacity remained constant over time. Because capacity can change with upgrades, major maintenance, or equipment deterioration, we rely instead on observed operating patterns to construct a time-varying measure of spare capacity.

last 12 months. Columns 1–4 show OLS estimates with log-transformed generation as the dependent variable, while columns 5–8 present PPML estimates using untransformed generation.

When we introduce the interaction between drought and high spare capacity (columns 2 and 6), we observe a significant pattern revealing important heterogeneity not captured by the baseline results (columns 1 and 5). The coefficient on drought becomes negative and significant in the OLS specification (-0.305), while the interaction term is positive and highly significant (0.642). The PPML results in column 6 show a similar pattern. These results reveal that plants with below-median spare capacity actually *reduce* generation during drought episodes, while those with above-median capacity significantly increase their generation. The negative coefficient on drought could reflect that water serves as an important input for thermal plants, either directly for cooling processes or indirectly through water-dependent fuel production, which makes some thermal generators vulnerable to drought conditions.

The coefficient on the high spare capacity indicator is positive and significant at the 1% level in both specifications. This likely reflects reversion to the mean in plant operations: plants with low recent generation relative to their maximum tend to generate more in subsequent periods, perhaps following maintenance periods or temporary shutdowns. Importantly, the positive interaction between drought and high capacity represents the additional effect during drought conditions, beyond this natural oscillation.

These results highlight that a plant's ability to respond to drought conditions depends critically on its available unused generation potential. Plants with greater flexibility to increase output play a crucial role in compensating for hydropower shortfalls during drought periods, while those with limited spare capacity may actually reduce generation, possibly because of operational constraints or strategic considerations related to the electricity market.

4.3.2 Local vs. System-Wide Drought Response

Having established how spare capacity affects drought response, we now examine whether thermal plants respond to local basin conditions, national conditions, or both—a distinction that reveals how transmission constraints may limit the system's ability to redistribute generation while also concentrating environmental impacts in drought-affected regions.

To capture national drought conditions, we construct a national drought index from a weighted average of local drought conditions across basins, where the weights reflect

each basin's share of total hydroelectric capacity. Specifically, we define a binary national drought indicator that equals one when the weighted drought measure exceeds a given threshold:

$$\text{natDrought}_t = \begin{cases} 1 & \text{if } \sum_b \omega_b \text{Drought}_{bt} > \tau, \\ 0 & \text{otherwise,} \end{cases}$$

where $\omega_b = \frac{\text{HydroCap}_b}{\sum_b \text{HydroCap}_b}$ represents basin b's share of total hydroelectric capacity. To determine the threshold τ, we examine the empirical distribution of the weighted drought measure. Figure 10 shows the frequency distribution of the weighted average of local droughts ($\sum_b \omega_b \text{Drought}_{bt}$). Most observations are clustered near zero (no drought), with a highly skewed distribution showing smaller clusters at higher drought intensity levels. We identify a natural break near 0.1, which we use as our threshold for identifying significant national drought events.[10]

Given that the potential response of thermal plants to drought conditions is likely determined by national drought conditions rather than local droughts alone, we estimate specifications that incorporate national drought measures. Since natDrought_t varies only at the time level, its main effect is absorbed by the market–time fixed effects α_{tm}, so we focus on its interaction with spare capacity:

$$\begin{aligned} \text{Generation}_{ibmt} = \beta_1(\text{natDrought}_t \times \text{Spare}_{ibt}) + \beta_2 \text{Spare}_{ibt} \\ + \mathbf{X}_{it}\gamma + \alpha_i + \alpha_{tm} + \varepsilon_{ibmt} \end{aligned} \tag{3}$$

where Spare_{ibt} is an indicator for plants with above-median spare capacity at the national level.

In Table 9, columns 3 and 7 present the OLS and PPML results for this specification, respectively. Column 3 shows that plants with spare capacity above the national median increase their generation by approximately 45.2% during national drought episodes (coefficient 0.452), with the effect being highly significant at the 1% level. The PPML estimate in column 7 shows a similar pattern, with a significant coefficient of 0.360.

In columns 4 and 8, we include interactions of both the local and national drought with plant capacity. The OLS results in column 4 show that plants with high capacity

[10]For the time-series evolution of the weighted national drought index, as well as its comparison with the simple (unweighted) average of local droughts, see Figure 6 in Section 3.

respond significantly to both types of drought conditions. The coefficient on the interaction between national drought and high capacity remains large and significant (0.369), while the interaction between local drought and high capacity is also significant (0.437). The PPML results in column 8 confirm this pattern, showing significant effects for the interactions of both national drought (0.320) and local drought (0.220) with high capacity.

Table 10 presents results using an alternative definition of spare capacity as measured over months $t-24$ to $t-13$ rather than the last 12 months. We observe similar patterns, but smaller magnitudes. In column 3, plants with high capacity increase generation by 26.9% during national droughts (in comparison to the increase of 45.2% we observe in Table 9). Examining both local and national drought effects simultaneously in column 4, we find that high-capacity plants increase generation by approximately 28% during local drought episodes (the combined effect of the drought coefficient and its interaction with high capacity) and by 36.9% during national drought periods (the coefficient on the national drought interaction). The PPML estimates in columns 7–8 remain robust, with coefficients of 0.358 and 0.372 on the national drought interaction. Interestingly, the local drought interaction term becomes insignificant in column 8 of Table 10 (-0.0343), suggesting that when historical capacity measures are used, plants respond primarily to national rather than local drought conditions.

These results collectively suggest that plants with high spare capacity play a crucial role in maintaining electricity supply during drought periods, with the strongest response observed when capacity is measured by recent (last 12 months') performance. The differential response to national and local drought conditions highlights how important it is to consider system-wide effects in analyzing how thermal plants compensate for hydroelectric shortfalls during drought episodes.

4.4 Environmental Implications of Thermal Substitution

A central motivation for this analysis is that drought-induced adjustments in the generation mix carry material environmental consequences. The evidence in Section 4.3 shows a systematic reallocation from hydropower to thermal production during drought episodes. We quantify the associated changes in power-sector emissions using observed fuel inputs at the plant–month level.

We compute plant-level CO_2 emissions from monthly fuel consumption data following the IPCC (2006) *Guidelines for National Greenhouse Gas Inventories*. For each fuel f,

plant i, and month t, emissions are given by

$$E_{ift} = Q_{ift} \times NCV_f \times EF_f,$$

where Q_{ift} is the reported fuel quantity, NCV_f the net calorific value (gigajoules [GJ] per unit), and EF_f the emission factor (kg CO_2 per GJ). We aggregate emissions across fuels at the plant–month level and divide by the number of days in each month to match the frequency of our generation data. All conversion factors are reported in Appendix Table A1.

We then estimate the response of emissions to drought shocks using the same econometric framework as in the generation analysis:

$$\text{Emissions}_{ibmt} = \beta_1(\text{natDrought}_t \times \text{Spare}_{ibt}) + \beta_2 \text{Spare}_{ibt} + \mathbf{X}_{it}\gamma + \alpha_i + \alpha_{tm} + \varepsilon_{ibmt}. \quad (4)$$

Here, Emissions_{ibmt} denotes the daily CO_2 emissions (tCO_2) of plant i in basin b, month m, and year t, natDrought_t captures national drought conditions, and Spare_{ibt} measures spare capacity at the plant level. The specification includes plant fixed effects (α_i) and market–month fixed effects (α_{tm}), as well as the same control vector $\mathbf{X}_{it}$ as in the generation regressions.

The coefficient on the interaction term ($\text{natDrought}_t \times \text{Spare}_{ibt}$) indicates that national droughts lead to higher emissions among plants with above-median spare capacity. Since PPML estimates a multiplicative model, the effect is measured as $\exp(\hat{\beta}) - 1$. For the preferred specification, $\hat{\beta} = 0.291$ implies an increase of about 33.8% in daily emissions, compared to a linear approximation of 29.1%. This magnitude closely parallels the generation response in Columns 1–2, confirming that the rise in emissions reflects greater utilization of idle thermal capacity rather than changes in efficiency.

To gauge the aggregate magnitude, we combine the estimated 33.8% increase with the number of plant–months in which national drought overlaps with above-median spare capacity ($PM_D = 894$), the median baseline level of daily emissions outside drought ($\overline{E}^{\text{base}} = 1{,}940$ tCO_2/day), and the average number of days per month (30.44). This corresponds to

$$\Delta E = 0.338 \times 1{,}940 \times 30.44 \times 894 \approx 17.9 \text{ MtCO}_2,$$

or about 1.09 $MtCO_2$ per year over the sample.

To contextualize this result, we can express the annual increment as a percentage of both the national and electricity-sector CO_2 emissions for Chile in benchmark years.

Considering official totals from the JRC and IEA (2025), the drought-driven increment represents 1.8% of national CO_2 and 6.5% of power industry emissions in 2005 and 1.4% and 5.5% in 2023 (see Table 12).

4.5 Drought and Investment Patterns

Our analysis thus far has focused on how existing power plants respond to drought conditions, revealing important patterns in how generation adjusts across plants with different technologies and capacity conditions. While these short-term responses are crucial for understanding the electricity system's resilience to weather shocks, they capture only adjustments along the intensive margin—how plants already in operation modify their output. In this section, we turn to adjustments on the extensive margin by examining how drought conditions influence investment decisions in new generation capacity.

Persistent droughts can reshape investment incentives in electricity markets by altering expected resource availability and the relative profitability of competing technologies. While short-run generation adjustments operate within existing capacity, investment decisions have important implications for both the future structure of the electricity system and its emissions trajectory, as drought-induced capacity additions may commit the system to specific generation technologies for decades. Whether droughts accelerate or delay the entry of new plants—and in which technologies—is ultimately an empirical question. This section examines how hydrological stress affects power plant entry across basins, emphasizing dynamic adjustments rather than contemporaneous correlations.

As a first step, we aggregate the plant-level dataset into a monthly basin panel and estimate two-way fixed effects (TWFE) models that relate prolonged drought spells to the number of operating plants. Formally, we estimate

$$Y_{btm} = \beta \, \text{Drought}_{bt} + \alpha_b + \alpha_t + \varepsilon_{btm}, \tag{5}$$

where Y_{btm} denotes the number of plants of technology m operating in basin b in month t, Drought_{bt} equals one when basin b is under a 36-month drought spell,[11] α_b denote basin fixed effects, and α_t denotes month–year fixed effects. This specification mirrors the high-frequency structure used in our generation analysis and provides a benchmark for assessing investment patterns at the basin level.

Figure 12 summarizes the association between 36-month drought spells and plant

[11] We use a 36-month cumulative drought measure to reflect the longer horizons relevant for investment decisions.

entry across technologies. The hydropower estimates (Panel (a)) are consistently negative across basin definitions, but none is statistically significant at the 10% level. The point estimates suggest modest negative effects, especially at the coarsest spatial aggregation, yet the wide confidence intervals prevent us from rejecting a zero effect. Thermal plants (Panel (b)) show positive and statistically significant responses that are stable across the alternative definitions. The estimates for Solar (Panel (c)) remain close to zero, with small and imprecise coefficients. The responses of wind (Panel (d)) are positive and statistically significant under most basin definitions, though the estimates become imprecise at the highest spatial resolution.

Because these static TWFE estimates reflect only contemporaneous correlations, they cannot capture anticipation, persistence, or the timing of investment responses. We therefore move to a staggered-adoption difference-in-differences (DID) design (Callaway and Sant'Anna, 2021), implemented on an annual basin panel, which recovers dynamic treatment effects relative to drought onset and quantifies long-run responses in a framework that is robust to heterogeneous treatment timing.

To study the dynamic response of investment to hydrological stress, we estimate an event–study design that traces basin-level plant entry before and after the onset of prolonged drought. $D_{b,t+k}$ is an indicator equal to one if basin b is k years from its first entry into a 36-month drought spell. We estimate

$$y_{bt} = \sum_{k=-5}^{-1} \beta_k D_{b,t+k} + \beta_0 D_{bt} + \sum_{k=1}^{10} \beta_k D_{b,t+k} + \mu_b + \tau_t + \varepsilon_{bt}, \tag{6}$$

where y_{bt} is the number of operating plants of a given technology in basin b and year t, and μ_b and τ_t denote basin and year fixed effects. We implement the design separately for hydropower, thermal, solar, and wind technologies and for three basin definitions (levels 06, 07, and 08), which enables us to assess sensitivity to spatial aggregation.

Table 13 reports the distribution of first drought onsets across basins, showing substantial dispersion in timing even though almost all the basins entered a drought at least once during 2005-–2024 (only one basin per aggregation level never meets the 36-month criterion). Most of the onsets occurred between 2013 and 2017, coinciding with the beginning of the megasequía, and this geographic and temporal staggering provides the timing variation required for the staggered-adoption DID estimator of Callaway and Sant'Anna (2021). Appendix Table A2 further shows that basins typically remain in drought for a large share of the months after onset, which underscores the persistence of these shocks.

Figure 13 reports event-study estimates of the response of plant entry to 36-month

drought spells. Across technologies, there is no evidence of differential pre-trends, and coefficients generally rise following drought onset. Thermal and wind display the clearest upward trajectories, with effects that strengthen over time and become statistically distinguishable from zero in the later post-treatment years; although thermal plants typically represent larger additions in installed capacity, their estimated entry dynamics are broadly similar in magnitude to those of wind. Solar shows a more muted and non-monotonic pattern, with imprecise positive estimates around treatment, a modest dip in the medium run, and positive coefficients toward the end of the window, consistent with delayed expansion. Hydropower, in contrast, exhibits no systematic response: point estimates drift upward in the long run, but wide confidence intervals prevent strong conclusions. These patterns are robust across HydroBASINS aggregation levels (Appendix Figures A5 and A6), which show qualitatively similar dynamics at finer spatial resolutions.

Because plants contribute very different amounts of capacity, we complement the plant-count analysis with installed capacity using the values reported in January 2025.[12] Figure A7 shows that installed capacity responds to drought in a pattern broadly consistent with the plant-count dynamics. Thermal capacity follows the same upward trajectory observed in the entry estimates, but with substantially wider confidence intervals. Wind and solar exhibit patterns that closely mirror those in plant counts, with positive and stable post-treatment dynamics across all spatial resolutions. Hydropower, by contrast, shows no adjustment at the coarsest resolution (level 06), where coefficients remain close to zero; as resolution increases (Appendix Figures A8 and A9), the estimates display a gradual upward drift and become statistically significant only in the final post-treatment periods for level 08. Taken together, these patterns indicate that capacity adjustments track the directional responses seen in plant entry, with thermal and nonconventional renewables showing consistent expansion, and hydropower exhibiting only marginal evidence of adjustment at finer spatial scales.

The evidence above shows that droughts induce investment shifts that reshape the generation mix. Thermal technologies expand most consistently and persistently in term of both plant entry and installed capacity, raising concerns about long-term lock-in of carbon-intensive technology. Wind and, with some delay, solar generation also increase following drought onset, indicating a parallel process of technological diversification. Hydropower responds the least, with small and imprecise adjustments that appear only in terms of capacity at the most disaggregated spatial levels. Overall, prolonged hydrological stress leads to an investment pattern combining diversification with a pronounced tilt

[12]Reported net effective capacity is available only for a single cross-section (January 2025), so we use these values as a time-invariant measure of plant size. This may miss historical upgrades or deterioration, but it provides a consistent metric to compare capacity adjustments across technologies.

toward thermal expansion.

5 Conclusion

This study provides comprehensive evidence on how drought conditions affected electricity generation systems in Chile from 2000 to 2024, revealing complex response dynamics that extend beyond direct impacts on hydropower production. Our findings demonstrate significant vulnerability in current electricity systems, with droughts reducing hydropower generation by approximately 24.5%. This substantial reduction highlights the inherent climate sensitivity of hydro-dependent systems such as Chile's, which face increasing challenges as drought conditions intensify.

To address this vulnerability, we find evidence of adaptation through thermal generation. Yet, this compensatory response is highly heterogeneous: thermal plants with above-median spare capacity increase generation by approximately 28% during local drought episodes, while those with limited capacity show no significant response or even reduce output. Importantly, high-capacity respond not only to local drought conditions but also to national ones, indicating drought lead to both local increases in emissions but also externalities to areas not directly affected by water scarcity. Such compensatory dynamics reveal a critical tension in electricity systems: adaptations that maintain short-term reliability may undermine longer-term climate sustainability.

Beyond these short-term operational shifts, we document that prolonged droughts are followed by increases in thermal capacity investments. This pattern suggests a feedback mechanism in which climate-induced water scarcity accelerates investment in carbon-intensive infrastructure, creating committed emissions that persist for decades. Such dynamics illustrate how repeated climate shocks may influence long-run energy system trajectories and complicate efforts to align resilience and sustainability objectives.

These results yield several critical policy implications. First, electricity system planning must explicitly account for rising drought risk under climate change scenarios, particularly in regions with high hydropower dependence. Second, our findings underscore the importance of diversification. Hydropower's sensitivity to droughts implies that it cannot, on its own, support a resilient low-carbon transition. Expanding the renewable portfolio, especially through solar and wind capacity, helps limit reliance on thermal plants while increasing resilience during water-scarcity. In parallel, expanding the geographic dispersion of generation assets reduces the system's exposure to localized climate shocks and supports system-wide resilience. Third, environmental and regulatory policies

should consider how market integration affects the spatial distribution of responses, since the location of drought-induced emissions may stay local but also be partially shifted toward plants located far from the affected basins. The environmental burden on the population therefore hinges on how thermal capacity and population are geographically distributed. Finally, policymakers should address the risk of future carbon lock-in from drought-induced investments in thermal capacity and develop strategies for managing existing assets to minimize committed emissions and stranded-asset risks.

As climate change intensifies drought frequency and severity globally, it is increasingly urgent that policymakers understand these complex dynamics to design resilient and sustainable electricity systems. Our analysis provides empirical foundations for anticipating how electricity systems might respond to increased water stress, with implications that extend beyond Chile to other regions with similar hydropower dependence and vulnerability to changing hydrological conditions. While the paper offers valuable evidence on the mechanisms linking droughts and electricity generation, several limitations point to avenues for future work. First, our analysis does not model welfare impacts of spatial shifts in thermal generation, nor demand-side adjustments, storage or transmission constraints. In addition, the relationship between drought conditions and investment patterns is observational and does not explore the complex market dynamics of plant entry. Future research should expand on this analysis along four dimensions. First, it should delve deeper into the effects of drought-induced shifts in generation on pollution and their welfare implications for populations, particularly highlighting geographic patterns in compensatory thermal production. This would shed light on an additional indirect pathway through which climate change may impact communities and potential externalities to communities not directly affected by droughts. Second, to understand the overall effects of droughts on the electricity systems, further work should delve into the impacts on other segments of the market, including generation of variable renewable energy, transmission and distribution efficiency, and storage options. Third, a clearer understanding of market dynamics concerning the entry and exit of generation plants could offer more precise insights on how the energy markets might react to changing weather patterns in the short and long term. Finally, replicating such analyses in other countries and contexts would help identify key determinants—such as geographic, climatic, infrastructure and institutional factors—that influence a market's response to droughts.

References

An, Y. and Zhang, L. (2023a). The thirst for power: The impacts of water availability on electricity generation in china. *The Energy Journal*, 44(2):205–240.

An, Y. and Zhang, X.-B. (2023b). The impact of water scarcity on electricity generation: Evidence from china. *Energy Economics*, 119:106640.

Bagnoli, L. S. and Cavallo, E. A., editors (2025). *From Risk to Reliability: Resilient Infrastructure Services to Face Nature's Challenges*. Inter-American Development Bank.

Bauer, C. J. (2009). Dams and markets: Rivers and electric power in chile. *Natural Resources Journal*, pages 583–651.

Callaway, B. and Sant'Anna, P. H. C. (2021). Difference-in-differences with multiple time periods. *Journal of Econometrics*, 225(2):200–230.

Center for Climate and Resilience Research (2021). Megasequía 2010-2018: Una lección para el futuro.

Cohen, S. M., Macknick, J., Averyt, K., and Meldrum, J. (2014). Modeling climate–water impacts on electricity sector capacity expansion. Technical report, National Renewable Energy Laboratory (NREL), U.S. Department of Energy. NREL/CP-6A20-61435.

Coordinador Eléctrico Nacional (2024). Histórico generación horaria por central. https://www.coordinador.cl/reportes-y-estadisticas. Accessed: 2024-02-01.

del Mar Rubio, M. and Tafunell, X. (2014). Latin american hydropower: A century of uneven evolution. *Renewable and Sustainable Energy Reviews*, 38:323–334.

Elliott, J. T. (2022). Investment, emissions, and reliability in electricity markets. Technical report, Working paper.

Eriksson, M., del Valle, A., and de la Fuente, A. (2025). Droughts worsen air quality and health by shifting power generation. *Nature Communications*, 16:4774.

Eyer, J. and Wichman, C. J. (2018). Does water scarcity shift the electricity generation mix toward fossil fuels? empirical evidence from the united states. *Journal of Environmental Economics and Management*, 87:224–241.

Fischer, R. and Galetovic, A. (2003). Regulatory governance and chile's 1998–1999 electricity shortage. *The Journal of Policy Reform*, 6(2):105–125.

Gaete-Morales, C., Gallego-Schmid, A., Stamford, L., and Azapagic, A. (2018). Assessing the environmental sustainability of electricity generation in chile. *Science of The Total Environment*, 636:1155–1170.

Gonzales, L. E., Ito, K., and Reguant, M. (2023). The investment effects of market integration: Evidence from renewable energy expansion in chile. *Econometrica*, 91(5):1659–1693.

González-Lorente, Á., Hernández-López, M., Martín-Álvarez, F. J., and Mendoza-Jiménez, J. (2024). A comparative analysis of electricity generation in Latin America and the Caribbean using multivariate techniques. *Heliyon*, 10(20):e39304.

Harris, L. (2024). Drought and investment in electricity markets. Working Paper.

Herrera-Estrada, J. E., Sheffield, J., and Diffenbaugh, N. S. (2018). Tracking the propagation of drought through the terrestrial water cycle. *Environmental Research Letters*, 13(8):084030.

Hunt, J. D., Stilpen, D., and de Freitas, M. A. V. (2018). A review of the causes, impacts and solutions for electricity supply crises in brazil. *Renewable and Sustainable Energy Reviews*, 88:208–222.

International Energy Agency (2021a). Climate impacts on latin American hydropower. Technical report, International Energy Agency, Paris.

International Energy Agency (2021b). Climate resilience: Electricity security 2021. Technical report, International Energy Agency. Accessed on December 16, 2024.

International Energy Agency (2024a). Weather for energy tracker. http://weatherforenergydata.iea.org. Accessed: 2024-02-01.

International Energy Agency (2024b). Weather for energy tracker: User's guide. Technical report, International Energy Agency.

JRC and IEA (2025). Edgar (emissions database for global atmospheric research) community ghg database, version edgar˙2025˙ghg. A collaboration between the European Commission Joint Research Centre (JRC) and the International Energy Agency (IEA), comprising IEA-EDGAR CO2, EDGAR CH4, EDGAR N2O, EDGAR F-Gases.

Lehner, B. and Grill, G. (2013). Global river hydrography and network routing: baseline data and new approaches to study the world's large river systems. *Hydrological Processes*, 27(15):2171–2186.

Moreno, J., Frohlich, V., and Gómez, C. (2024). Progress achieved in the retirement of coal facilities in chile and the definition of a just energy transition strategy. Technical report, Deutsche Gesellschaft für Internationale Zusammenarbeit (GIZ). Case Study.

Pollitt, M. (2004). Electricity reform in chile. lessons for developing countries. *Journal of Network Industries*, os-5(3-4):221–262.

Qiu, M., Ratledge, N., Azevedo, I. M., Diffenbaugh, N. S., and Burke, M. (2023). Drought impacts on the electricity system, emissions, and air quality in the western united states. *Proceedings of the National Academy of Sciences*, 120(28):e2300395120.

Ralston Fonseca, F., Craig, M., Jaramillo, P., Bergés, M., Severnini, E., Loew, A., Zhai, H., Cheng, Y., Nijssen, B., Voisin, N., and Yearsley, J. (2021). Effects of climate change on capacity expansion decisions of an electricity generation fleet in the southeast u.s. *Environmental Science & Technology*, 55(4):2522–2531.

Serra, P. (2022). Chile's electricity markets: Four decades on from their original design. *Energy Strategy Reviews*, 39:100798.

Van Vliet, M. T., Sheffield, J., Wiberg, D., and Wood, E. F. (2016). Impacts of recent drought and warm years on water resources and electricity supply worldwide. *Environmental Research Letters*, 11(12):124021.

Vega-Coloma, M. and Zaror, C. A. (2018). Environmental impact profile of electricity generation in chile: A baseline study over two decades. *Renewable and Sustainable Energy Reviews*, 94:154–167.

Yalew, S. G., Hirpa, F. A., Ambelu, A., Taye, M. T., and van Griensven, A. (2020). A review of water-energy-food nexus methodologies. *Environmental Research Letters*, 15(12).

Ömer Karaduman (2021). Large scale wind power investment's impact on wholesale electricity markets. Working Paper 2021-020, MIT CEEPR.

Figures

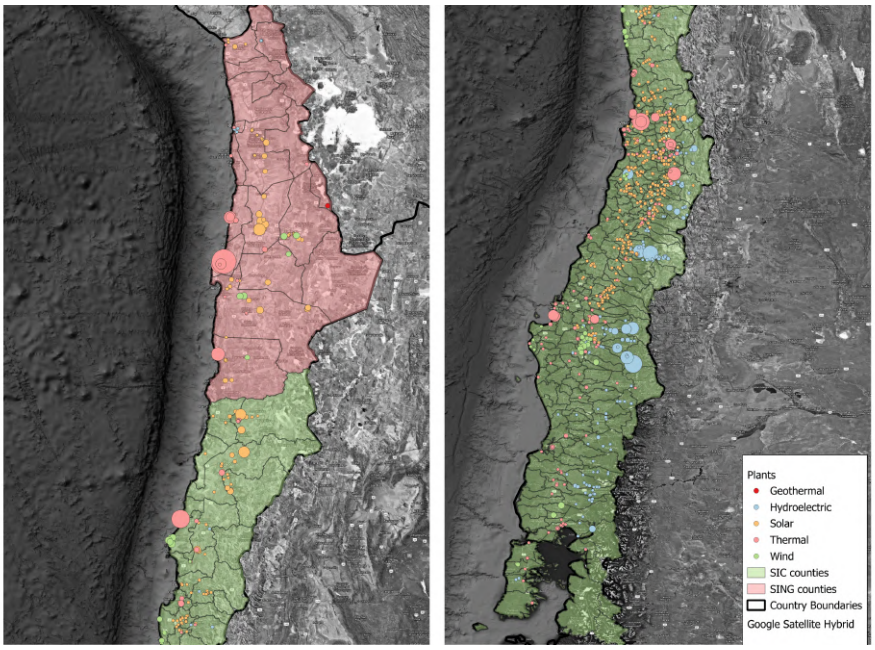

Figure 1: Plants by Technology and Size

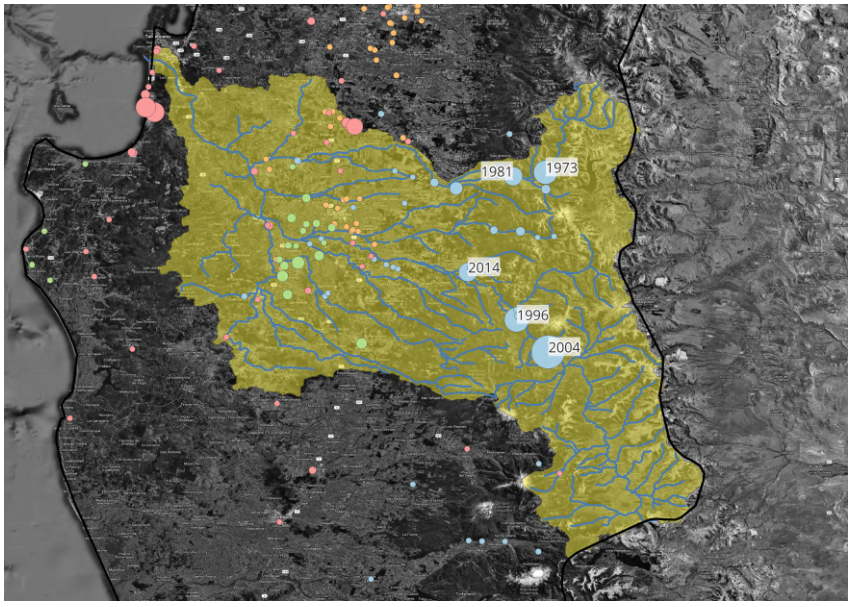

Figure 2: Hydroplants in Bío Bío River Basin

Figure 3: Evolution of Electricity Generation by Technology Type (2000–2024)

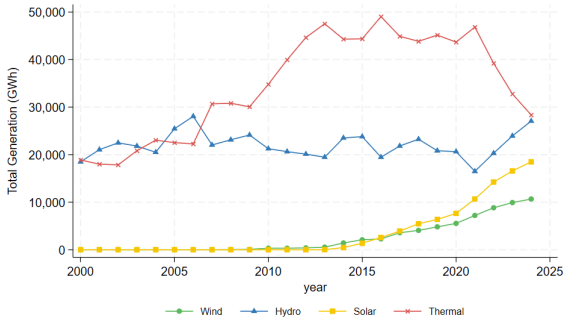

(a) Total Generation

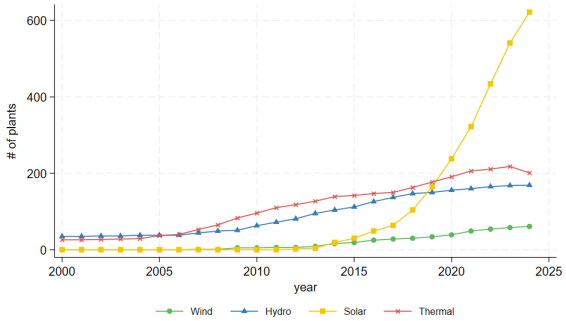

(b) Number of Plants

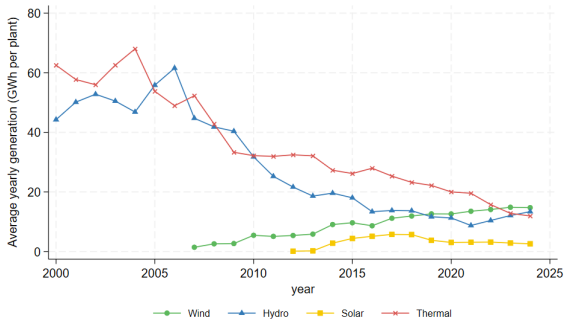

(c) Average Generation per Plant

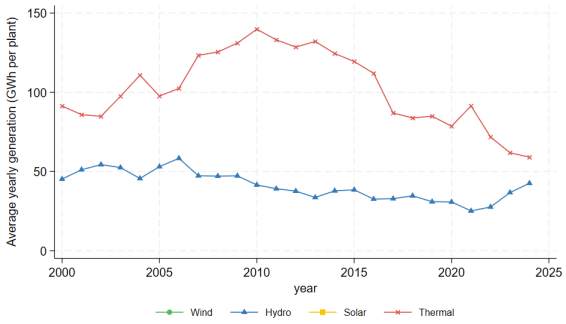

(d) Average Generation (Plants Active in 2000)

Source: Authors' own calculation based on Coordinador Eléctrico Nacional (2024). See details in Section 3.1
Note: Panel (a) shows total electricity generation by technology type. Panel (b) displays the number of plants by technology. Panel (c) presents the average generation per plant across all plants. Panel (d) shows the average generation for only those plants already active in 2003, highlighting production trends independent of new entry effects.

Figure 4: Generation and Plant Numbers in Former SING and SIC (2000-2024)

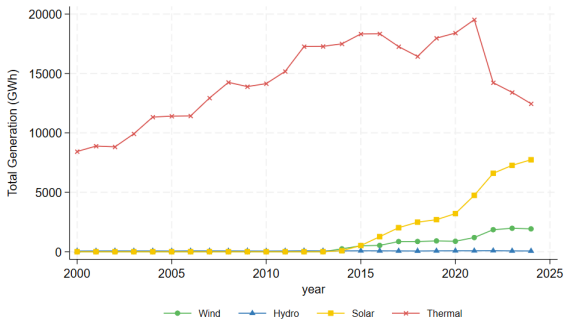

(a) Total Generation (Former SING)

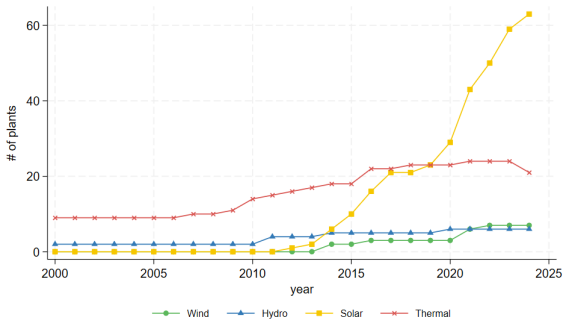

(b) Number of Plants (Former SING)

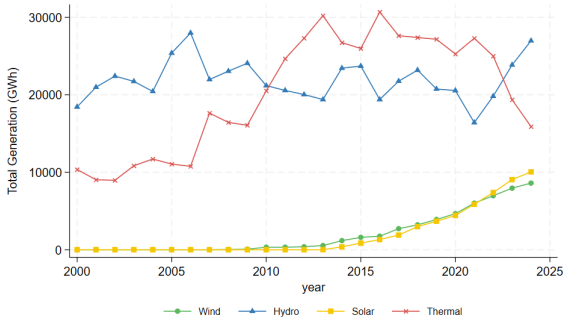

(c) Total Generation (Former SIC)

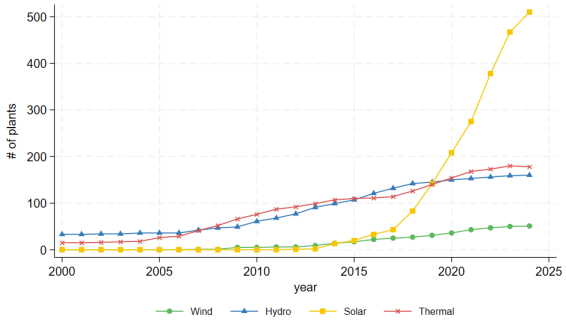

(d) Number of Plants (Former SIC)

Source: Authors' own calculation based on Coordinador Eléctrico Nacional (2024). See details in Section 3.1
Note: This figure illustrates the distinct evolution of Chile's two main power systems. The top row shows the northern SING, characterized by minimal hydropower, stable thermal generation, and early solar adoption due to desert conditions. The bottom row shows the southern SIC, with its historically dominant hydropower, increased thermal generation after 2010 during the megasequía, and more balanced renewable mix featuring both wind and solar. Panels (a) and (c) show total generation by technology, while Panels (b) and (d) display the number of plants by technology type.

Figure 5: Evolution of Hydropower Generation by Plant Type and Vintage (2000–2025)

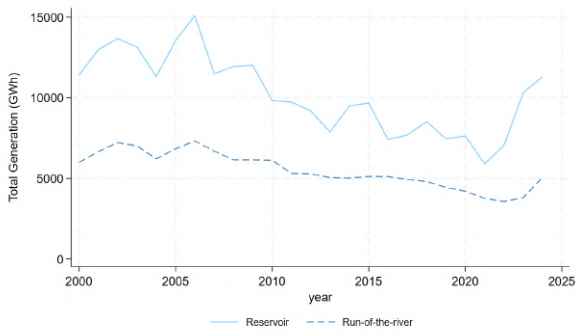

(a) Generation from plants active in 2000

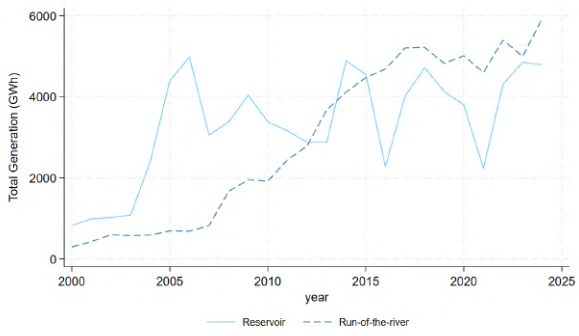

(b) Generation from plants added since 2000

Note: This figure contrasts generation from established versus new hydropower plants during Chile's drought period. Panel (a) illustrates how existing plants faced challenges, with pre-2000 reservoir plants declining from approximately 15,000 GWh to 6,000 GWh (2005-2020) before showing partial recovery. Panel (b) demonstrates how sector expansion occurred primarily through new run-of-river installations, which grew steadily from near zero to approximately 6,000 GWh by 2025, offsetting some of the losses from established plants.

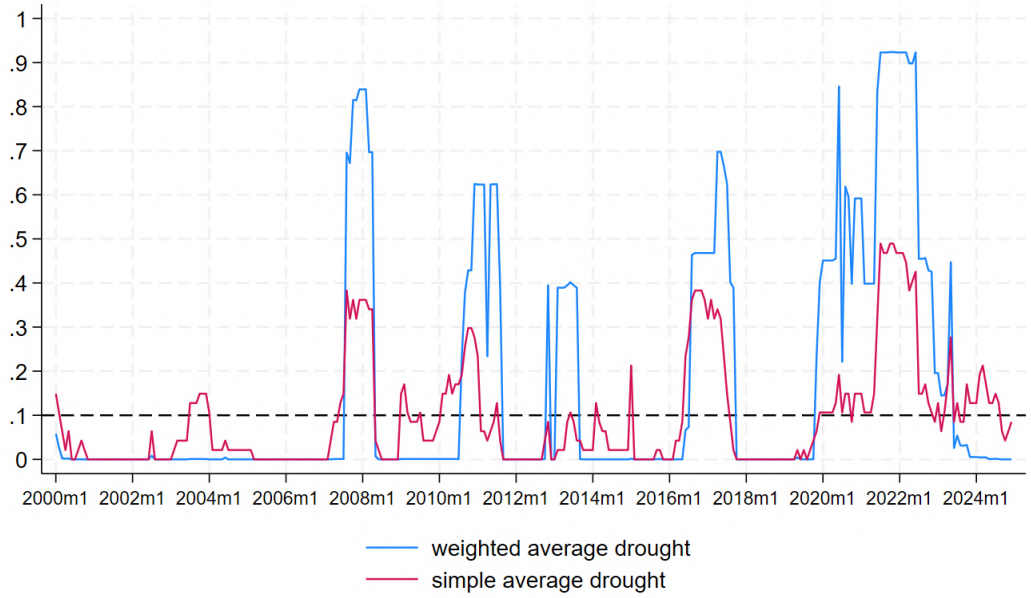

Figure 6: Evolution of Drought (2000–2024)

Note: The national drought index is the weighted share of basins in drought, where weights reflect each basin's share of total hydroelectric capacity. This aggregation gives greater influence to droughts occurring in hydropower-relevant basins. For reference, the figure also shows the simple (unweighted) average drought incidence and the 0.1 threshold used in the construction of the national drought indicator.

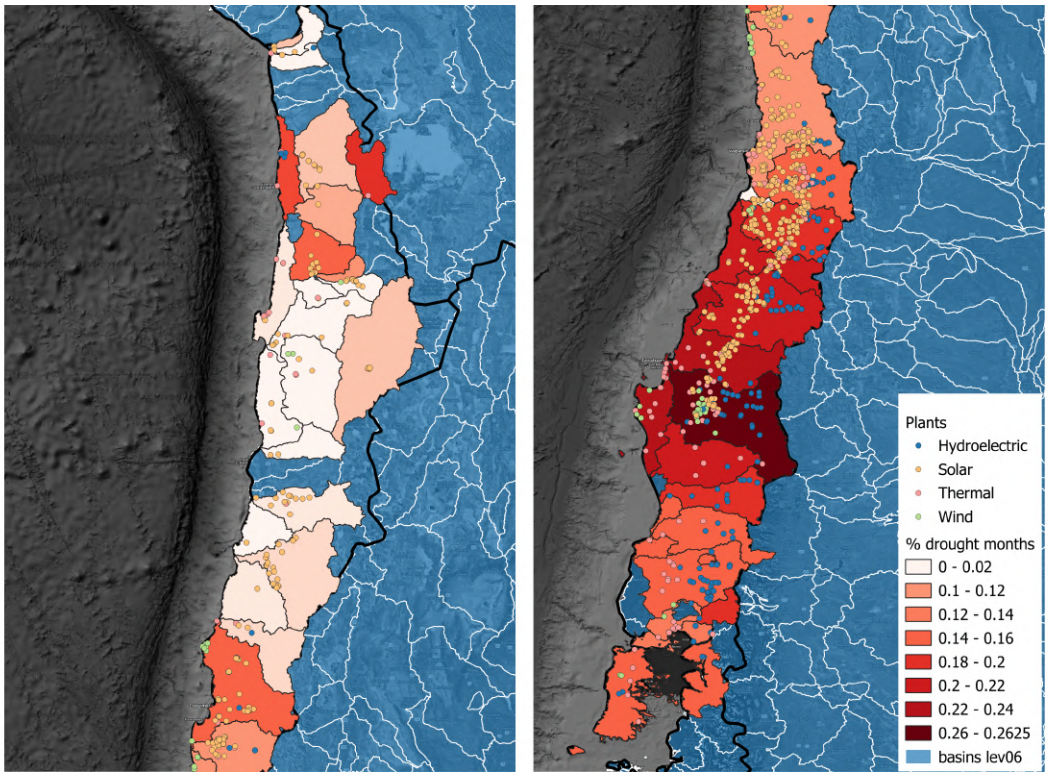

Figure 7: Geographical Distribution of Drought (2005–2024)

Note: The figure reports, for each HydroBASINS Level 06 unit, the percentage of months in drought over our analysis window (January 2005–December 2024), with power plants overlaid by technology.

Figure 8: Impact of Drought on Electricity Generation by Technology Type

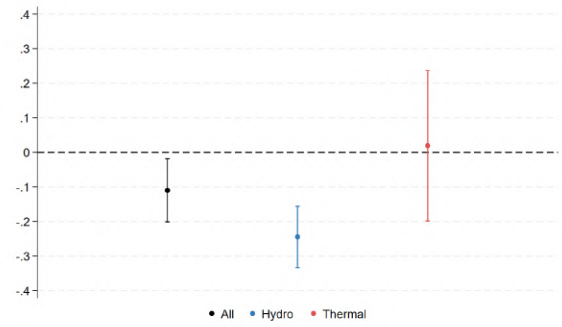

(a) Hydro and Thermal (2005–2024)

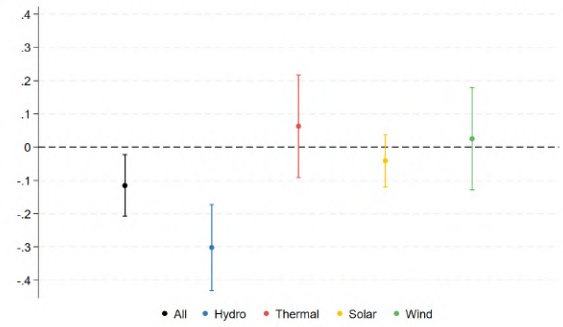

(b) All Technologies (2015–2024)

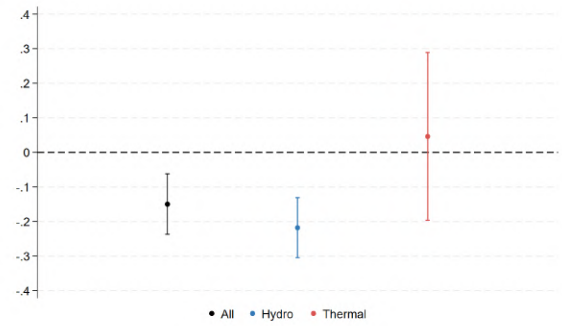

(c) SIC Only, Hydro and Thermal (2005–2024)

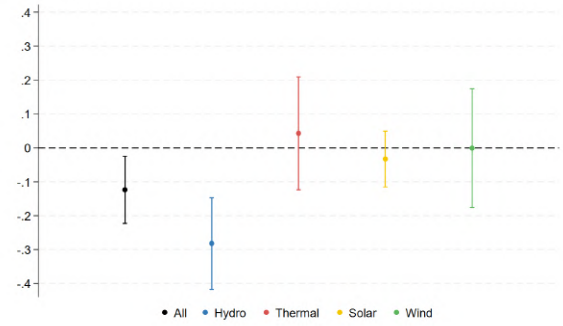

(d) SIC Only, All Technologies (2015–2024)

Note: This figure shows the coefficients from our preferred specification (with full meteorological controls) for different technology types. Error bars represent 95% confidence intervals. Panels (a) and (b) show results for all markets using hydro and thermal only (2005–2024) and for all technology types (2015–2024), respectively. Panels (c) and (d) restrict the sample to the SIC market for the same technology groupings and time periods.

Figure 9: Temporal Patterns of Drought Effects on Thermal and Hydroelectric Generation

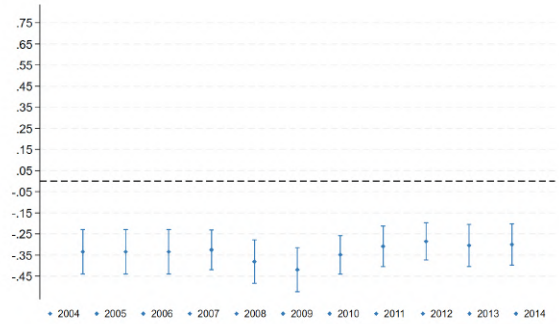

(a) Hydropower plants, Cohort Robustness

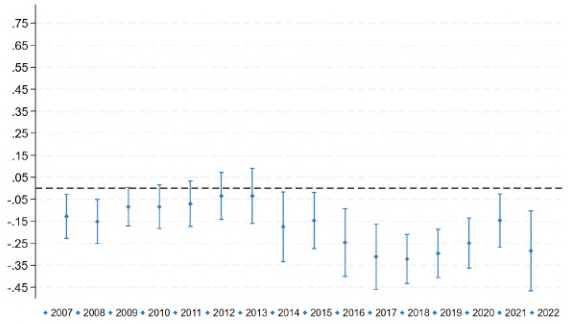

(b) Hydropower plants, 5-Year Rolling Windows

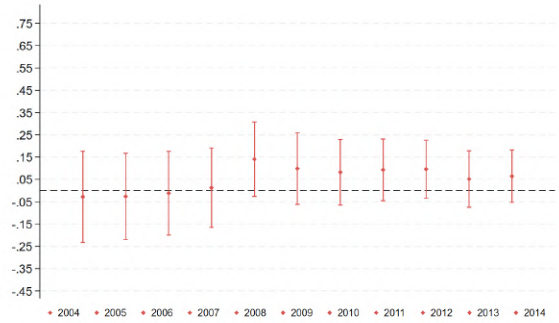

(c) Thermal Plants, Cohort Robustness

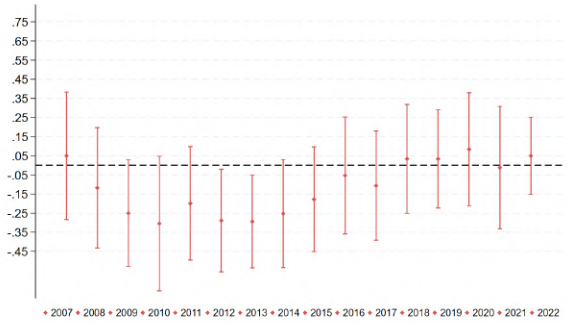

(d) Thermal Plants, 5-Year Rolling Windows

Notes: This figure shows the estimated coefficients for the effect of drought on electricity generation. Panels (a) and (c) test robustness to sample selection by fixing the analysis period (2015–2024) while varying the plant cohorts included. Each point estimate represents plants that began operation in or before the year indicated. Panels (b) and (d) show estimates from 5-year rolling windows for plants that began operation before 2005, with the year label indicating the midpoint of each window. Red markers (Panels (a) and (b)) represent thermal plants, while blue markers (Panels (c) and (d)) represent hydropower plants. The dashed horizontal line at zero represents no effect. Vertical bars indicate 95% confidence intervals. All specifications include plant fixed effects, time fixed effects, and full meteorological controls.

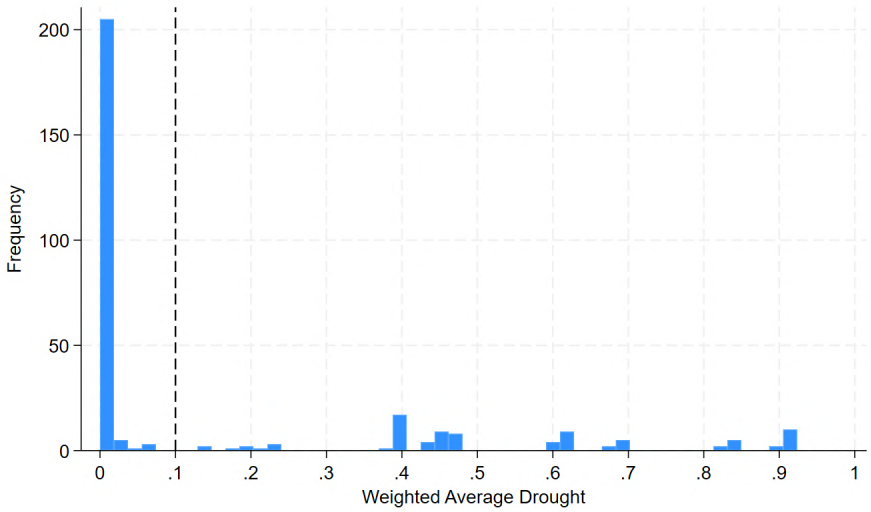

Figure 10: Distribution of the Weighted National Drought Index (2000–2024)

Note: The figure shows the distribution of the weighted national drought index over 2000–2024. Most observations cluster near zero, with a long right tail corresponding to high-intensity drought episodes. The vertical dashed line at 0.1 denotes the threshold used to define national drought conditions.

Figure 11: Drought and Entry of New Plants (2001–2024)

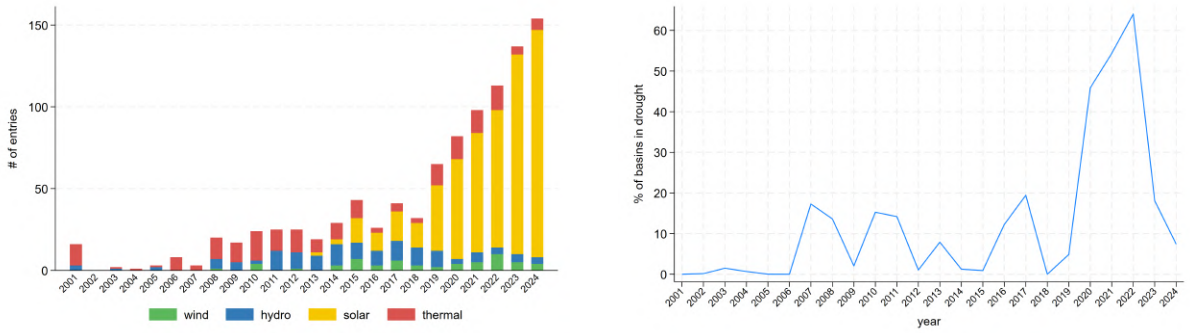

(a) Plant Entries by Technology

(b) 12-Month Drought Conditions

Note: This figure illustrates the temporal relationship between power plant investments and drought conditions. Panel (a) shows the entry of new power plants by technology type (solar, wind, thermal, hydro) over time. Panel (b) displays the percentage of basins experiencing drought conditions at level 06 using a 12-month measure. Key periods include the initial drought increase around 2007, the gradual technology transition from 2008-2014, and the dramatic shift from 2019 onward with increased drought prevalence coinciding with accelerated solar investment and some thermal power resurgence.

Figure 12: Two-Way Fixed Effects Estimates: Drought and Power Plant Entry

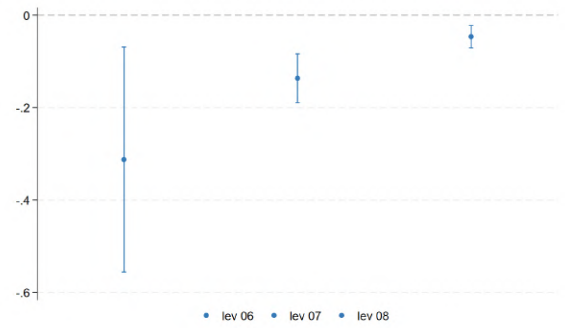

(a) Hydropower Plants

(b) Thermal Plants

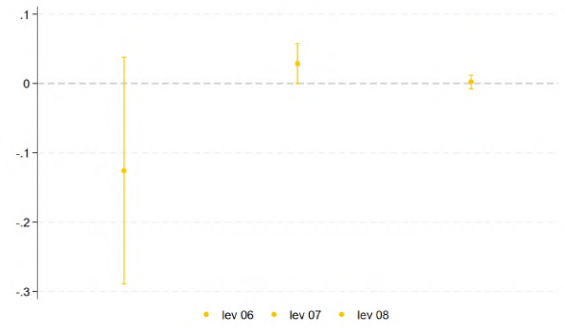

(c) Solar Plants

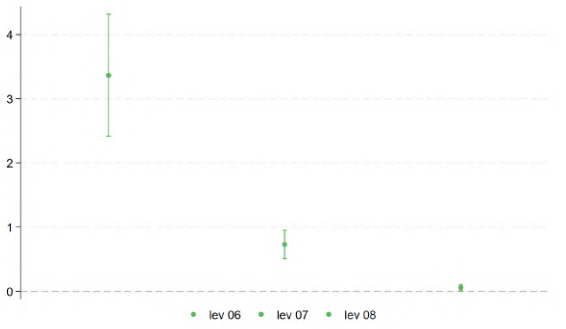

(d) Wind Plants

Notes: Each panel reports estimates from basin-level regressions of the number of operating plants on a 36-month drought indicator. All specifications include basin and year fixed effects, and standard errors are clustered at the basin level. Vertical bars denote 90% confidence intervals. The sample includes all basins within the SIC that ever host hydropower generation, and outcomes are reported from 2005 onward.

Figure 13: Dynamic Effects of Drought on Plant Entry (Number of Plants)

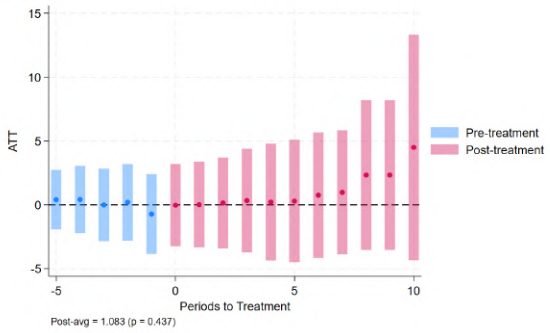

(a) Hydropower

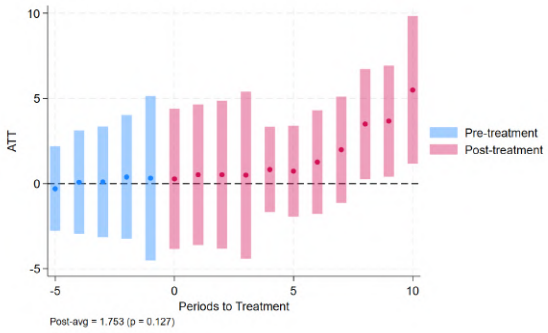

(b) Thermal

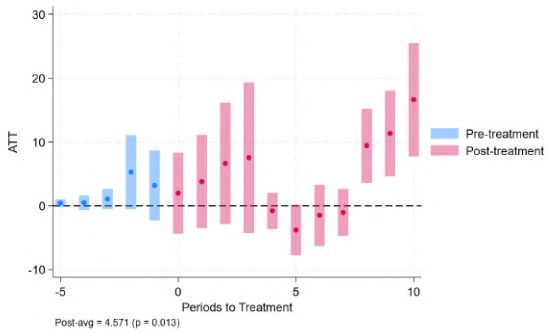

(c) Solar

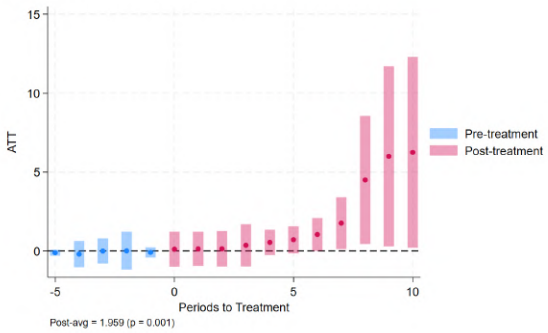

(d) Wind

Notes: Each panel reports dynamic treatment effects of 36-month drought spells on the number of operating plants, estimated using the staggered-adoption difference-in-differences estimator of Callaway and Sant'Anna (2021). The horizontal axis measures years relative to the first drought spell in each basin; the vertical axis reports average treatment effects on the treated (ATT). Blue (red) bars denote pre-treatment (post-treatment) periods; vertical bars indicate 90% confidence intervals. The sample includes all SIC basins that ever host hydropower generation. This figure reports results for HydroBASINS Level 06.

Tables

Table 1: Hydropower Plants by Type and Activity in 2000

	Active in 2000	**Inactive in 2000**	**Total**
Reservoir	8 (4.88%)	3 (1.83%)	11 (6.71%)
Non-Reservoir	24 (14.63%)	129 (78.66%)	153 (93.29%)
Total	32 (19.51%)	132 (80.49%)	164 (100.00%)

Notes: This table presents the distribution of hydropower plants by type (reservoir and nonreservoir) and activity status in 2000. Percentages of the total sample are shown in parentheses.

Table 2: Summary Statistics

Panel (a): All Plants

	count	mean	min	p50	max
Capacity	1124	34.01	0.0100	5.424	980.1
Market (1 in SIC, 0 in SING)	1127	0.819	0	1	1
Active in 2000	1127	0.0521	0	0	1
Commissioning Year	1119	2015.7	1909	2020	2024

Panel (b): Thermal Plants

	count	mean	min	p50	max
Capacity	234	65.65	0.181	6.094	980.1
Market (1 in SIC, 0 in SING)	235	0.796	0	1	1
Active in 2000	235	0.102	0	0	1
Commissioning Year	232	2009.8	1939	2011	2024

Panel (c): Hydro Plants

	count	mean	min	p50	max
Capacity	181	41.53	0.104	5.473	685.1
Market (1 in SIC, 0 in SING)	182	0.929	0	1	1
Active in 2000	182	0.190	0	0	1
Commissioning Year	182	2003.8	1909	2013	2024

Panel (d): Wind

	count	mean	min	p50	max
Capacity	61	78.94	5.150	62.95	205.2
Market (1 in SIC, 0 in SING)	62	0.823	0	1	1
Active in 2000	62	0	0	0	0
Commissioning Year	61	2018.1	2007	2020	2024

Panel (e): Geo

	count	mean	min	p50	max
Capacity	1	83.58	83.58	83.58	83.58
Market (1 in SIC, 0 in SING)	1	0	0	0	0
Active in 2000	1	0	0	0	0
Commissioning Year	1	2019	2019	2019	2019

Panel (f): Solar

	count	mean	min	p50	max
Capacity	647	16.14	0.0100	3	401.1
Market (1 in SIC, 0 in SING)	647	0.798	0	1	1
Active in 2000	647	0	0	0	0
Commissioning Year	643	2020.9	2012	2021	2024

Notes: This table presents summary statistics for electricity generation plants in our sample by source type. Panel (a) includes all plants, while Panels (b)–(f) present statistics for specific source types. Capacity refers to net effective capacity reported by the system operator, based on the January 2025 extraction that reflects the end of our sample period.

Table 3: Impact of Droughts on Overall Electricity Generation

	(1)	(2)	(3)	(4)	(5)	(6)	(7)
drought	-0.149***	-0.159***	-0.153***	-0.145***	-0.141***	-0.155***	-0.154***
	(-4.03)	(-4.36)	(-4.15)	(-3.96)	(-3.84)	(-4.24)	(-4.24)
temperature		0.107***					0.0798***
		(10.29)					(5.97)
humididty			0.00752***				0.00334
			(4.52)				(1.27)
precipitation				0.583***			0.798***
				(4.46)			(4.39)
windspeed					0.241***		0.156**
					(3.93)		(2.22)
pressure						0.00164***	0.00150***
						(12.76)	(9.33)
Observations	13742	13742	13742	13742	13742	13742	13742
# plants	65	65	65	65	65	65	65
# months	240	240	240	240	240	240	240
# basins	19	19	19	19	19	19	19

Notes: $*p < 0.10, **p < 0.05, ***p < 0.01$. t-statistics in parentheses. All regressions include plant fixed effects and market-specific time (month–year) fixed effects. The dependent variable is daily electricity generation (MWh). Standard errors are clustered at the basin × period level.

Table 4: Impact of Droughts on Hydropower Generation

	(1)	(2)	(3)	(4)	(5)	(6)	(7)
drought	-0.233***	-0.248***	-0.240***	-0.227***	-0.224***	-0.242***	-0.245***
	(-6.45)	(-6.95)	(-6.78)	(-6.47)	(-6.33)	(-6.79)	(-7.05)
temperature		0.132***					0.0971***
		(11.64)					(6.63)
humididty			0.0144***				0.00971***
			(9.26)				(3.94)
precipitation				1.009***			0.867***
				(8.50)			(4.55)
windspeed					0.390***		0.195**
					(4.88)		(2.08)
pressure						0.00185***	0.00143***
						(14.73)	(8.89)
Observations	8714	8714	8714	8714	8714	8714	8714
# plants	38	38	38	38	38	38	38
# months	240	240	240	240	240	240	240
# basins	12	12	12	12	12	12	12

Notes: $*p < 0.10, **p < 0.05, ***p < 0.01$. t-statistics in parentheses. All regressions include plant fixed effects and market-specific time (month–year) fixed effects. The dependent variable is daily electricity generation (MWh). Standard errors are clustered at the basin × period level.

Table 5: Impact of Droughts on Thermal Generation

	(1)	(2)	(3)	(4)	(5)	(6)	(7)
drought	0.0130	0.0117	0.0211	0.00496	0.0180	0.0117	0.0230
	(0.15)	(0.14)	(0.25)	(0.06)	(0.21)	(0.14)	(0.27)
temperature		0.0232					-0.0268
		(0.92)					(-0.86)
humididty			-0.0140***				-0.0145*
			(-2.83)				(-1.82)
precipitation				-1.251***			-0.530
				(-2.61)			(-0.85)
windspeed					0.0952		0.104
					(0.99)		(0.97)
pressure						0.000491	0.000716
						(1.04)	(1.25)
Observations	5028	5028	5028	5028	5028	5028	5028
# plants	27	27	27	27	27	27	27
# months	240	240	240	240	240	240	240
# basins	13	13	13	13	13	13	13

Notes: $*p < 0.10, **p < 0.05, ***p < 0.01$. t-statistics in parentheses. All regressions include plant fixed effects and market-specific time (month–year) fixed effects. The dependent variable is daily electricity generation (MWh). Standard errors are clustered at the basin × period level.

Table 6: Impact of Droughts on Solar Generation

	(1)	(2)	(3)	(4)	(5)	(6)	(7)
drought	-0.0418	-0.0417	-0.0422	-0.0433	-0.0423	-0.0402	-0.0391
	(-1.35)	(-1.36)	(-1.37)	(-1.41)	(-1.38)	(-1.31)	(-1.29)
temperature		0.0297***					0.0257**
		(4.48)					(2.07)
humididty			-0.00397***				-0.000836
			(-3.48)				(-0.40)
precipitation				-0.820***			-0.174
				(-4.09)			(-0.62)
windspeed					-0.0247		0.0238
					(-0.40)		(0.32)
pressure						0.000433	0.000689
						(0.93)	(1.36)
Observations	1972	1972	1972	1972	1972	1972	1972
# plants	19	19	19	19	19	19	19
# months	120	120	120	120	120	120	120
# basins	8	8	8	8	8	8	8

Notes: $*p < 0.10, **p < 0.05, ***p < 0.01$. t-statistics in parentheses. All regressions include plant fixed effects and market-specific time (month–year) fixed effects. The dependent variable is daily electricity generation (MWh). Standard errors are clustered at the basin × period level.

Table 7: Impact of Droughts on Wind Generation

	(1)	(2)	(3)	(4)	(5)	(6)	(7)
drought	-0.0382	-0.0316	-0.0381	-0.0375	0.0165	-0.0358	0.0262
	(-0.62)	(-0.51)	(-0.62)	(-0.61)	(0.28)	(-0.58)	(0.44)
temperature		-0.0220					-0.0390**
		(-1.50)					(-2.06)
humididty			0.000220				-0.00221
			(0.09)				(-0.56)
precipitation				0.282			0.348
				(0.89)			(0.75)
windspeed					0.522***		0.553***
					(11.88)		(11.06)
pressure						-0.000223	0.000481**
						(-1.44)	(2.10)
Observations	1911	1911	1911	1911	1911	1911	1911
# plants	16	16	16	16	16	16	16
# months	120	120	120	120	120	120	120
# basins	8	8	8	8	8	8	8

Notes: $*p < 0.10, **p < 0.05, ***p < 0.01$. t-statistics in parentheses. All regressions include plant fixed effects and market-specific time (month-year) fixed effects. The dependent variable is daily electricity generation (MWh). Standard errors are clustered at the basin × period level.

Table 8: Comparison of OLS (log) and PPML Estimates

	All Plants		Hydro Only		Thermal Only	
	(1)	(2)	(3)	(4)	(5)	(6)
	OLS (log)	PPML	OLS (log)	PPML	OLS (log)	PPML
drought	-0.154***	-0.0839***	-0.245***	-0.191***	0.0230	0.0385
	(-4.24)	(-3.79)	(-7.05)	(-7.80)	(0.27)	(1.09)
Observations	13742	15541	8714	9120	5028	6421
# plants	65	65	38	38	27	27
# months	240	240	240	240	240	240
# basins	19	19	12	12	13	13

Notes: $*p < 0.10, **p < 0.05, ***p < 0.01$. t-statistics in parentheses. All regressions include plant fixed effects and market-specific time (month–year) fixed effects. The dependent variable is monthly average daily electricity generation. Odd-numbered columns use OLS with log-transformed dependent variable, while even-numbered columns use Poisson Pseudo-Maximum Likelihood (PPML) estimation. Columns 1–2 include all plants, columns 3–4 include hydro plants only, and columns 5–6 include thermal plants. Standard errors are clustered at the basin × period level.

Table 9: Thermal Response to Droughts – Spare Capacity in Last 12 Months

	OLS (log)				PPML (level)			
	(1)	(2)	(3)	(4)	(5)	(6)	(7)	(8)
drought	0.0230	-0.305**		-0.159	0.0385	-0.290***		-0.144
	(0.26)	(-2.56)		(-1.20)	(1.03)	(-3.04)		(-1.48)
drought x spare		0.642***		0.437***		0.374***		0.220**
		(4.58)		(2.83)		(3.78)		(2.16)
nat drought x spare			0.452***	0.369***			0.360***	0.320***
			(4.78)	(3.48)			(5.94)	(4.89)
spare		0.815***	0.718***	0.707***		0.318***	0.225***	0.218***
		(8.92)	(7.47)	(7.39)		(8.75)	(5.81)	(5.62)
Observations	5028	5028	5028	5028	6421	6421	6421	6421
# plants	27	27	27	27	27	27	27	27
# months	240	240	240	240	240	240	240	240
# basins	13	13	13	13	13	13	13	13
controls	yes	yes	yes	yes	yes	yes	yes	yes

Notes: $*p < 0.10, **p < 0.05, ***p < 0.01$. t-statistics in parentheses. All regressions include plant fixed effects and market-specific time (month–year) fixed effects. Columns 1–4 present OLS estimates with log-transformed daily electricity generation as the dependent variable, while columns 5–8 present PPML estimates with daily electricity generation (MWh) as the dependent variable. Spare capacity is calculated with generation data from the last 12 months. Standard errors are clustered at the basin × period level.

Table 10: Thermal Response to Droughts – Spare Capacity in Previous 12 Months

	OLS (log)				PPML (level)			
	(1)	(2)	(3)	(4)	(5)	(6)	(7)	(8)
drought	0.0230	-0.181		-0.103	0.0385	-0.0845		0.0858
	(0.26)	(-1.45)		(-0.75)	(1.03)	(-1.03)		(0.99)
drought x spare		0.433***		0.321**		0.148*		-0.0343
		(2.90)		(1.97)		(1.68)		(-0.37)
nat drought x spare			0.269***	0.208**			0.358***	0.372***
			(2.81)	(1.97)			(5.49)	(5.36)
spare		0.458***	0.415***	0.404***		0.259***	0.184***	0.184***
		(4.91)	(4.33)	(4.22)		(7.30)	(5.15)	(5.16)
Observations	5028	5022	5022	5022	6421	6414	6414	6414
# plants	27	27	27	27	27	27	27	27
# months	240	240	240	240	240	240	240	240
# basins	13	13	13	13	13	13	13	13
controls	yes	yes	yes	yes	yes	yes	yes	yes

Notes: $*p < 0.10, **p < 0.05, ***p < 0.01$. t-statistics in parentheses. All regressions include plant fixed effects and market-specific time (month–year) fixed effects. Columns 1–4 present OLS estimates with log-transformed daily electricity generation as the dependent variable, while columns 5–8 present PPML estimates with daily electricity generation (MWh) as the dependent variable. Spare capacity is calculated with generation data from months $t-24$ to $t-13$. Standard errors are clustered at the basin × period level.

Table 11: Thermal Response to Droughts: Generation and Emissions

	Spare capacity: Last 12 months (t–1 to t–12)			Spare capacity: Prev. 12 months (t–13 to t–24)		
	Generation (MWh)		Emissions (tCO_2)	Generation (MWh)		Emissions (tCO_2)
	(1)	(2)	(3)	(4)	(5)	(6)
nat drought x high cap	0.381***	0.512***	0.291***	0.331***	0.431***	0.209***
	(5.35)	(5.45)	(4.04)	(4.31)	(4.85)	(2.86)
high cap	0.216***	0.181***	0.276***	0.111***	0.0404	0.119**
	(4.99)	(3.35)	(5.19)	(2.91)	(0.85)	(2.53)
Observations	5285	4146	4146	5285	4146	4146
# plants	27	26	26	27	26	26
# months	197	197	197	197	197	197
# basins	13	13	13	13	13	13
Sample	All	Restricted to emis. sample		All	Restricted to emis. sample	

Notes: $*p < 0.10$, $**p < 0.05$, $***p < 0.01$. t-statistics in parentheses. All columns report PPML estimates. Columns 1–3 use spare capacity defined over the last twelve months ($t-1$ to $t-12$), while columns 4–6 use spare capacity defined over the previous twelve months ($t-13$ to $t-24$). For the dependent variable, columns 1, 2, 4, and 5 use daily electricity generation (MWh), and columns 3 and 6 use daily emissions (tCO_2). Columns 1 and 4 use all available plant-month observations in periods with emissions data; columns 2, 3, 5, and 6 are restricted to the sample used in the emissions regressions (i.e., plants and months with valid emission measurements). All regressions include plant fixed effects and market-specific time (month–year) fixed effects. Standard errors are clustered at the basin × month level.

Table 12: Magnitude of drought-driven thermal emissions

	National total ($MtCO_2$/yr)	**Share of national CO_2 (%)**	**Power industry total ($MtCO_2$/yr)**	**Share of power industry CO_2 (%)**
2005	59.14	1.84%	16.78	6.50%
2023	77.01	1.41%	19.96	5.46%

Notes: National and power industry CO_2 emissions for Chile in 2005 and 2023 are taken from the EDGAR Community GHG Database (JRC and IEA, 2025). Percentage columns report the contribution of the back-of-the-envelope annualized increment of 1.09 $MtCO_2$/yr, based on the median baseline of 1,940 tCO_2/day and the realized $PM_D = 894$. Using the mean baseline (2,300 tCO_2/day) yields a slightly higher increment of 1.29 $MtCO_2$/yr (2.2–1.7% of national and 7.7–6.5% of power industry emissions).

Table 13: Distribution of First Drought Entries

Year	Hybas06	Hybas07	Hybas08
Never	1	1	1
2008	0	1	1
2012	0	2	3
2013	3	14	26
2014	1	2	2
2015	2	0	0
2016	0	1	4
2017	5	6	7
2019	0	1	1
2020	0	0	1
2021	9	10	14
2022	0	6	17
Total basins	21	44	77

Notes: Each cell reports the number of basins (b) entering drought for the first time in a given year, using the 36-month drought definition. "Never" indicates basins that do not enter drought during 2005–2024.

A Appendix

A.1 Figures

Figure A1: Hydro Generation Response to Drought (Basin Level Variations)

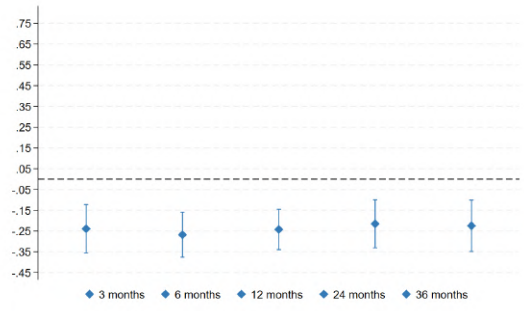

(a) Basin Level 04

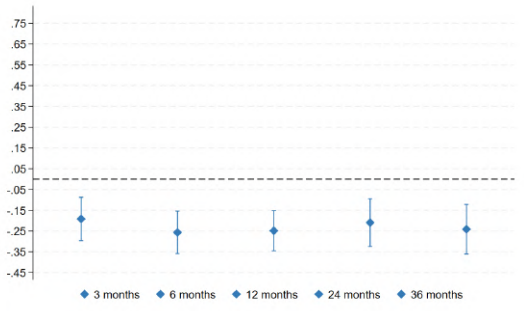

(b) Basin Level 05

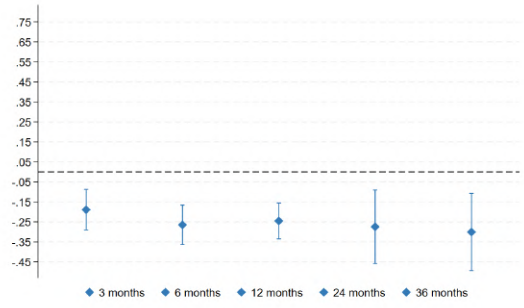

(c) Basin Level 06 (Baseline)

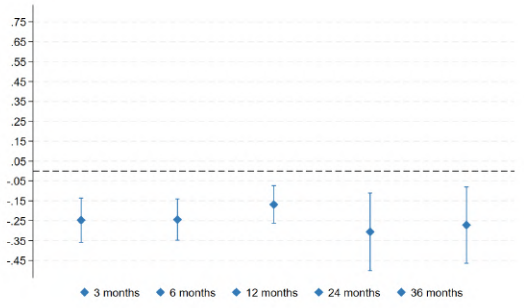

(d) Basin Level 07

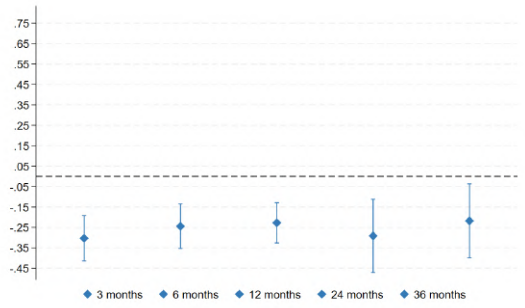

(e) Basin Level 08

Note: This figure shows coefficient estimates and 95% confidence intervals for the effect of drought on hydroelectric generation, varying the basin level while keeping the 12-month accumulation period constant. All specifications include plant fixed effects, time fixed effects, and plant-specific controls.

Figure A2: Thermal Generation Response to Drought (Basin Level Variations)

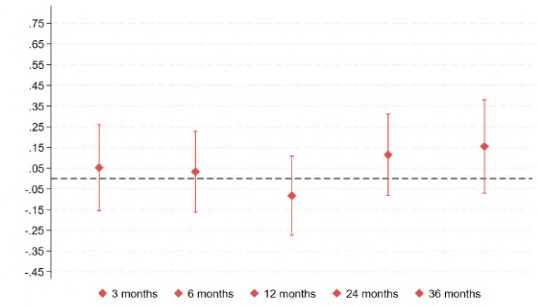

(a) Basin Level 04

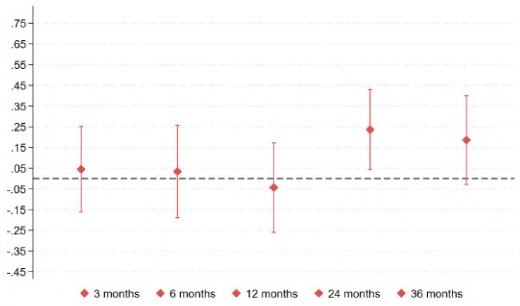

(b) Basin Level 05

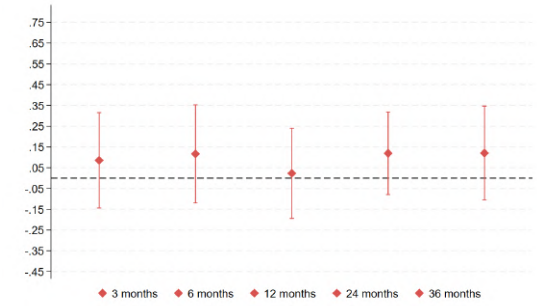

(c) Basin Level 06 (Baseline)

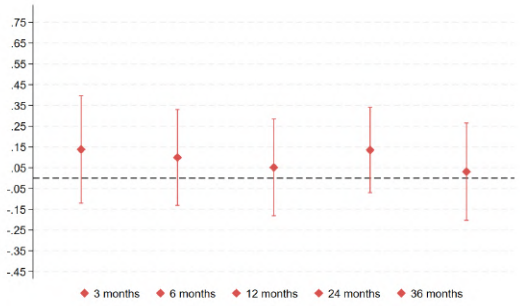

(d) Basin Level 07

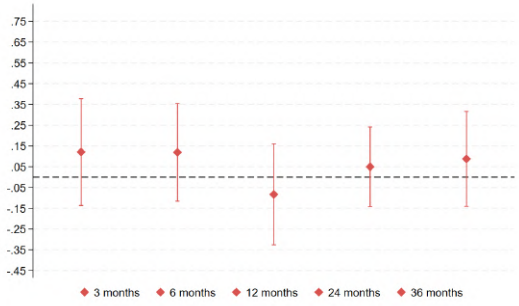

(e) Basin Level 08

Note: This figure shows coefficient estimates and 95% confidence intervals for the effect of drought on thermal generation, varying the basin level while keeping the 12-month accumulation period constant. All specifications include plant fixed effects, time fixed effects, and plant-specific controls.

Figure A3: Hydro Generation Response to Drought (Time Variations)

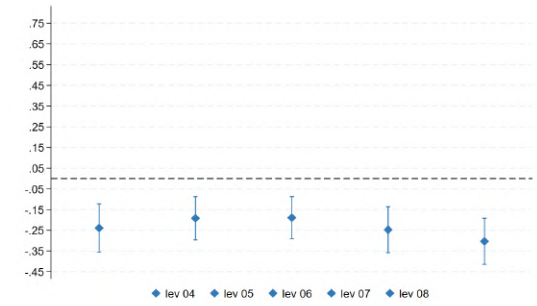

(a) 3-Month Accumulation

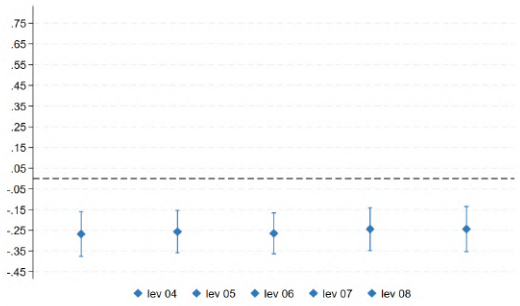

(b) 6-Month Accumulation

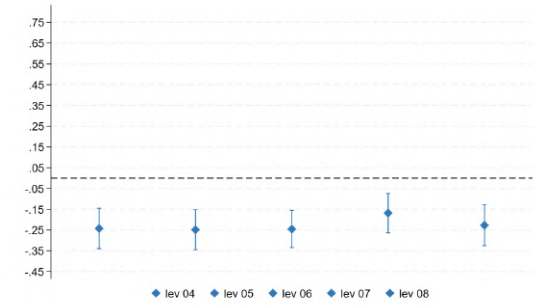

(c) 12-Month Accumulation (Baseline)

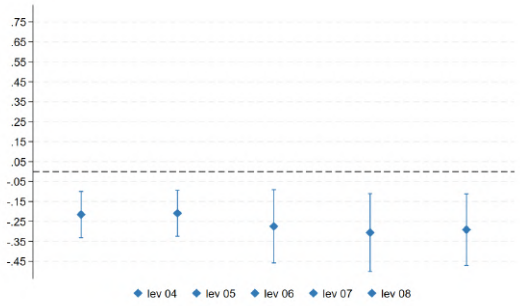

(d) 24-Month Accumulation

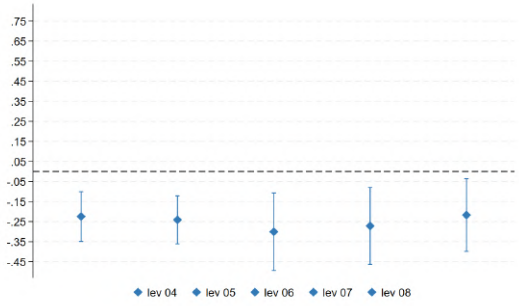

(e) 36-Month Accumulation

Note: This figure shows coefficient estimates and 95% confidence intervals for the effect of drought on hydroelectric generation, varying the temporal accumulation period while keeping the basin level constant at 06. All specifications include plant fixed effects, time fixed effects, and plant-specific controls.

Figure A4: Thermal Generation Response to Drought (Time Variations)

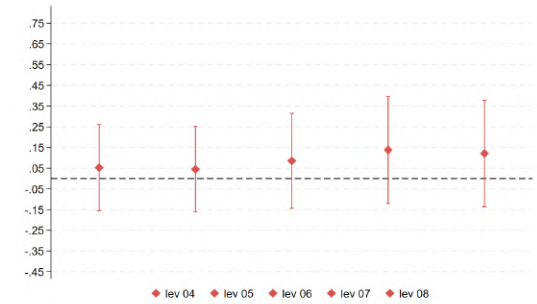

(a) 3-Month Accumulation

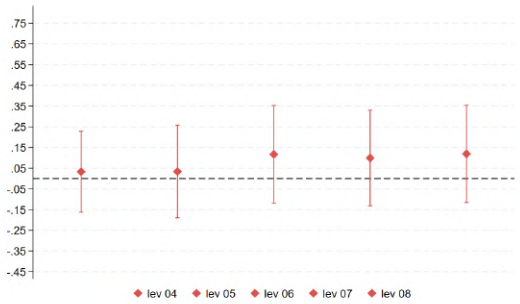

(b) 6-Month Accumulation

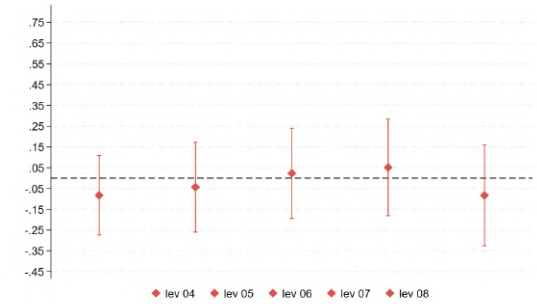

(c) 12-Month Accumulation (Baseline)

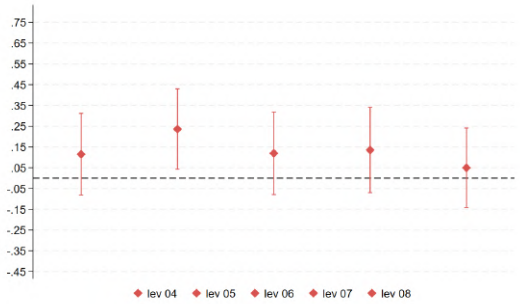

(d) 24-Month Accumulation

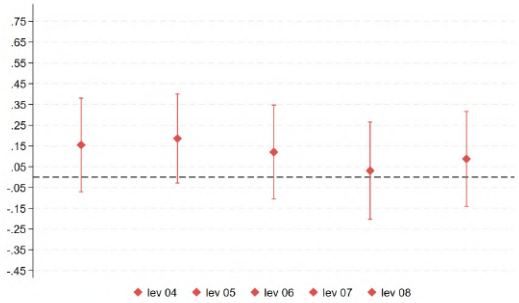

(e) 36-Month Accumulation

Note: This figure shows coefficient estimates and 95% confidence intervals for the effect of drought on thermal generation, varying the temporal accumulation period while keeping the basin level constant at 06. All specifications include plant fixed effects, time fixed effects, and plant-specific controls.

Figure A5: Dynamic Effects of Drought on Plant Entry (Level 07)

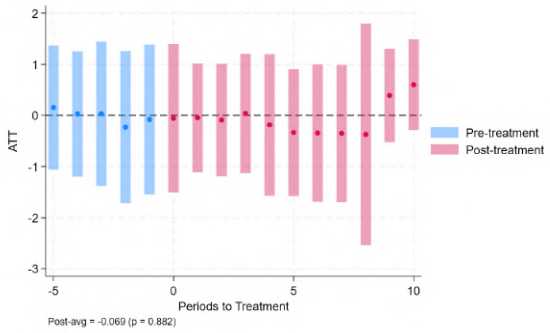

(a) Hydropower

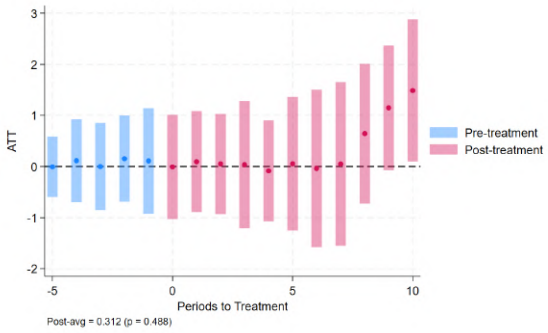

(b) Thermal

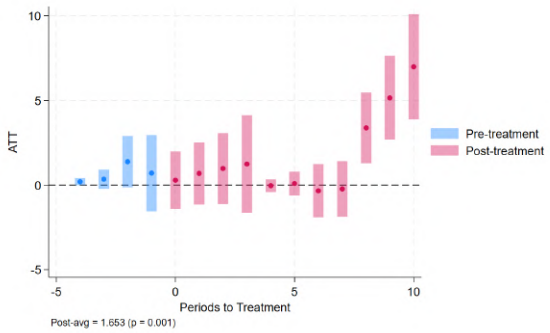

(c) Solar

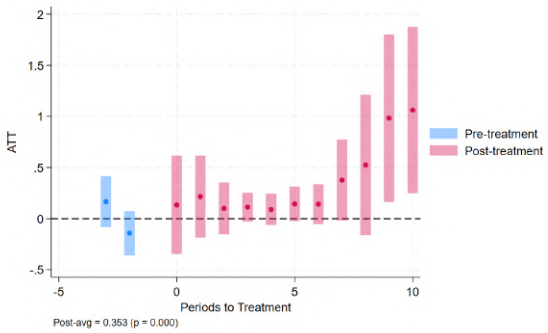

(d) Wind

Notes: Each panel reports dynamic treatment effects of 36-month drought spells on the number of operating plants, estimated using the staggered-adoption difference-in-differences estimator of Callaway and Sant'Anna (2021). The horizontal axis measures years relative to the first drought spell in each basin; the vertical axis reports average treatment effects on the treated (ATT). Blue (red) bars denote pre-treatment (post-treatment) periods; vertical bars indicate 90% confidence intervals. The sample includes all SIC basins that ever host hydropower generation. This figure reports results for HydroBASINS Level 07.

Figure A6: Dynamic Effects of Drought on Plant Entry (Level 08)

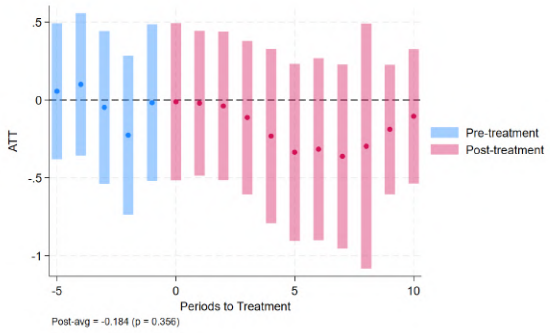

(a) Hydropower

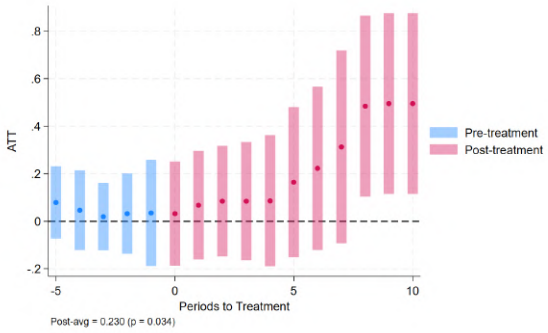

(b) Thermal

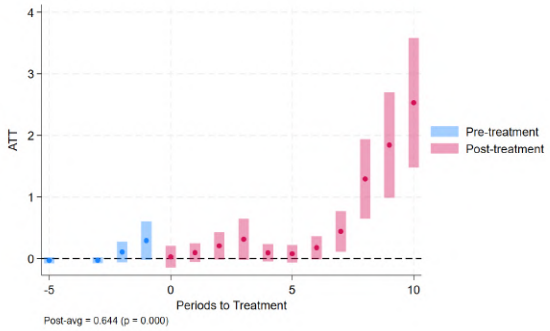

(c) Solar

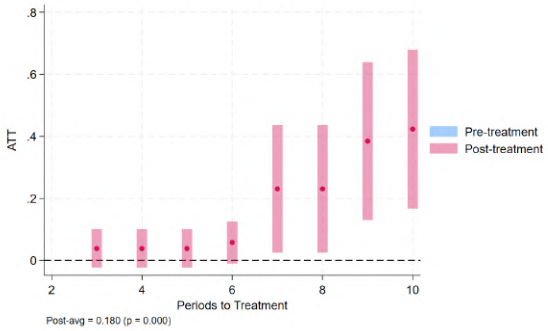

(d) Wind

Notes: Each panel reports dynamic treatment effects of 36-month drought spells on the number of operating plants, estimated using the staggered-adoption difference-in-differences estimator of Callaway and Sant'Anna (2021). The horizontal axis measures years relative to the first drought spell in each basin; the vertical axis reports average treatment effects on the treated (ATT). Blue (red) bars denote pre-treatment (post-treatment) periods; vertical bars indicate 90% confidence intervals. The sample includes all SIC basins that ever host hydropower generation. This figure reports results for HydroBASINS Level 08.

Figure A7: Dynamic Effects of Drought on Installed Capacity (Level 06)

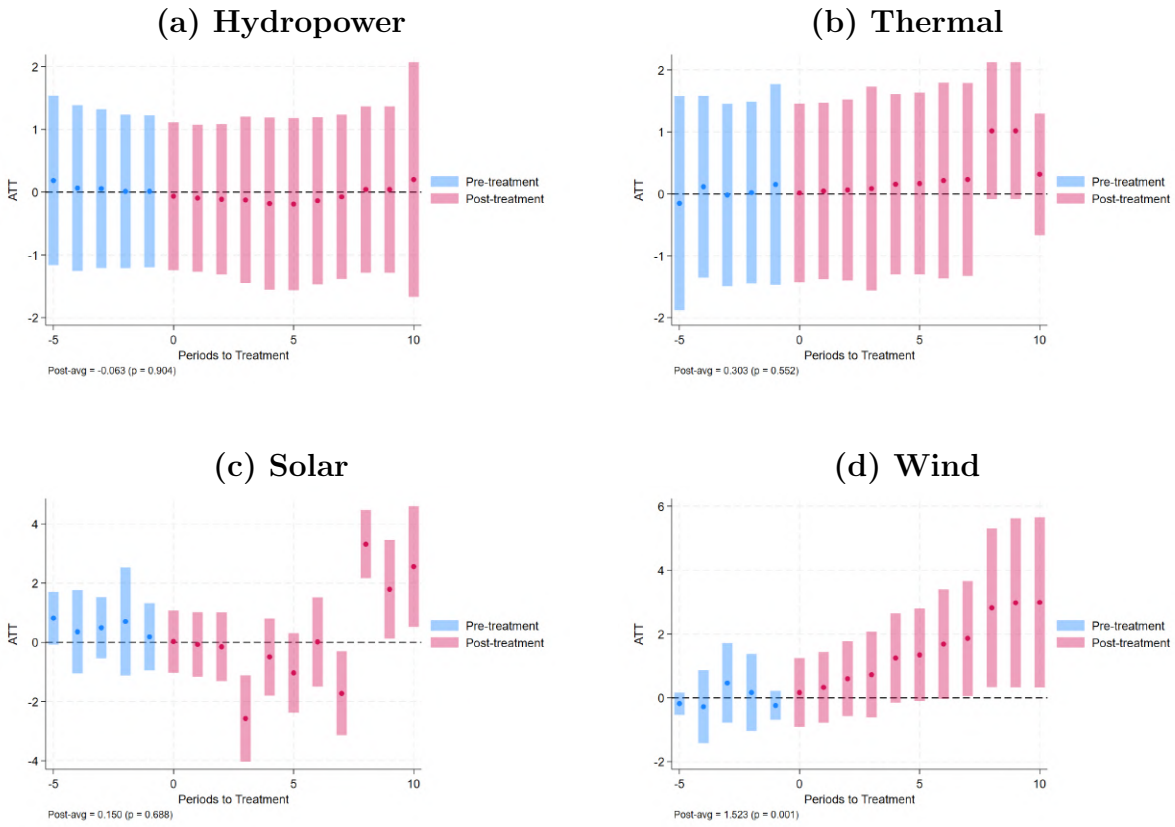

Notes: Each panel reports dynamic treatment effects of 36-month drought spells on installed capacity (asinh–transformed), estimated using the staggered-adoption difference-in-differences estimator of Callaway and Sant'Anna (2021). The horizontal axis measures years relative to first drought entry. Vertical bars denote 90% confidence intervals. The sample includes all SIC basins that ever host hydropower generation; outcomes are measured annually.

Figure A8: Dynamic Effects of Drought on Installed Capacity (Level 07)

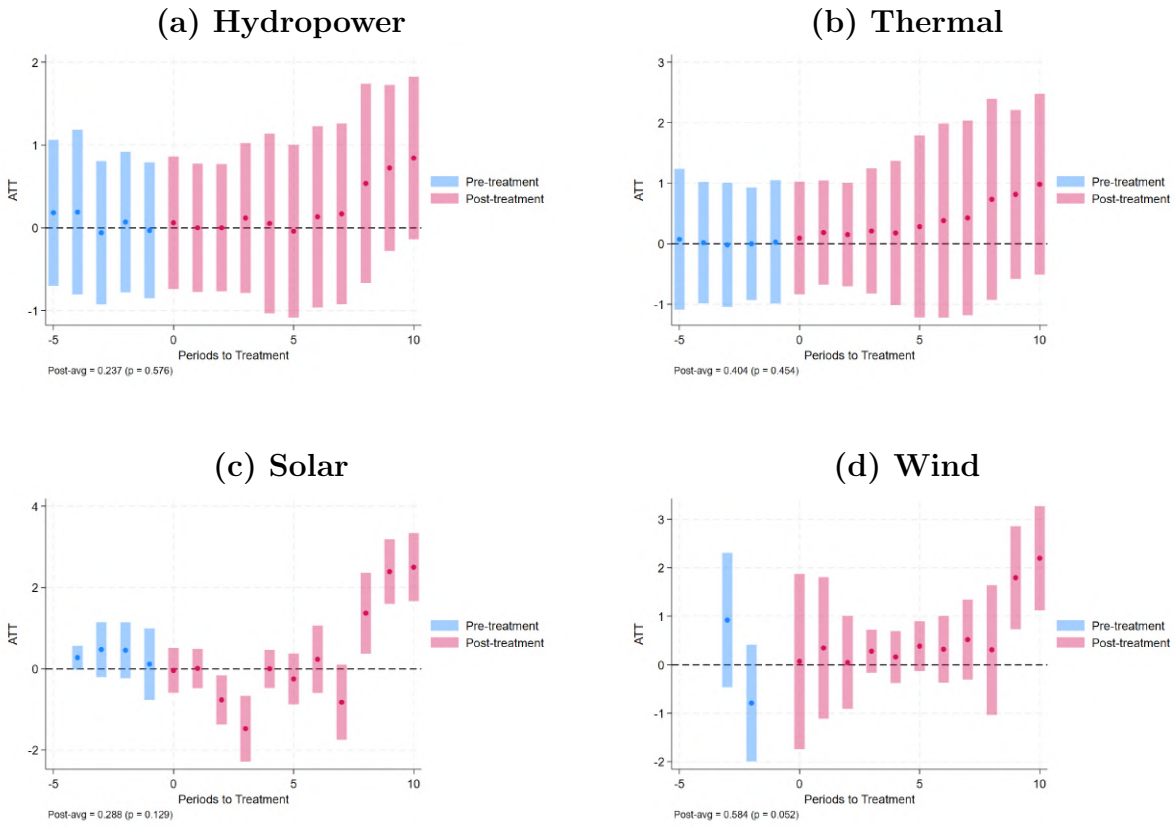

Notes: Each panel reports dynamic treatment effects of 36-month drought spells on installed capacity (asinh–transformed), estimated using the staggered-adoption difference-in-differences estimator of Callaway and Sant'Anna (2021). The horizontal axis measures years relative to first drought entry. Vertical bars denote 90% confidence intervals. The sample includes all SIC basins that ever host hydropower generation; outcomes are measured annually.

Figure A9: Dynamic Effects of Drought on Installed Capacity (Level 08)

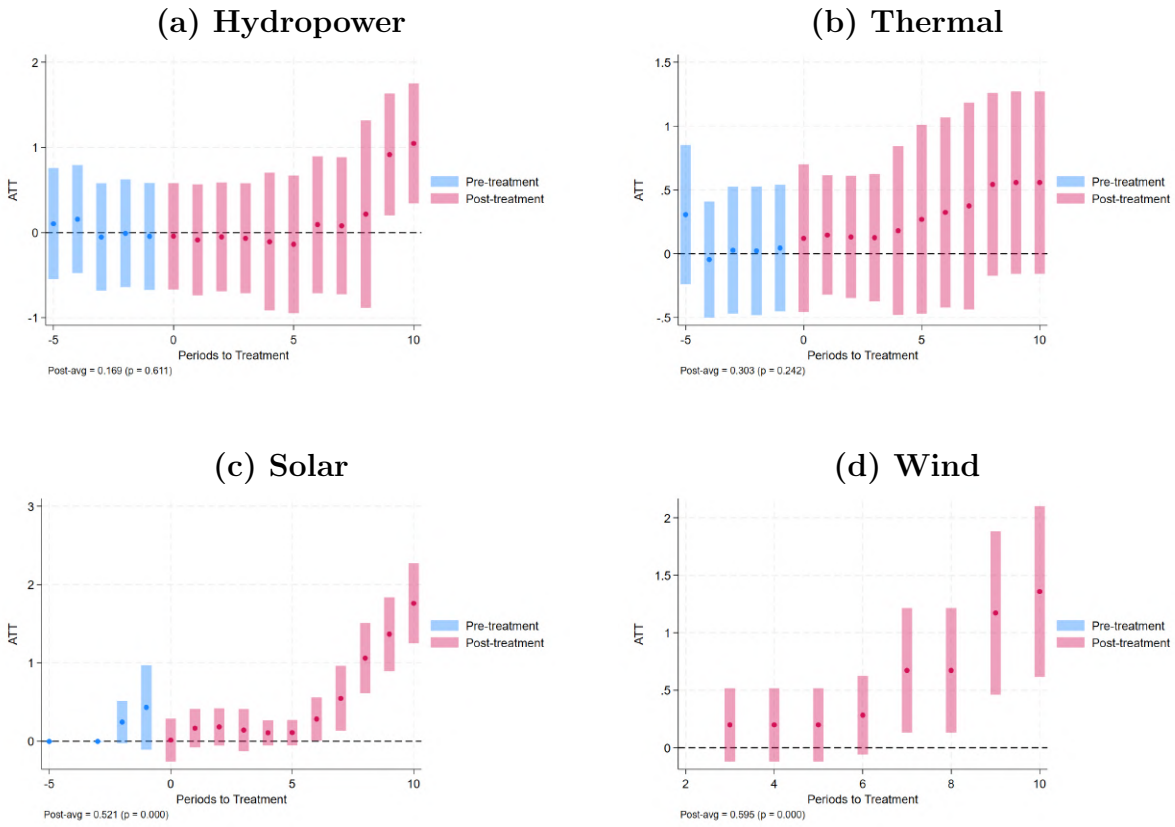

Notes: Each panel reports dynamic treatment effects of 36-month drought spells on installed capacity (asinh–transformed), estimated using the staggered-adoption difference-in-differences estimator of Callaway and Sant'Anna (2021). The horizontal axis measures years relative to first drought entry. Vertical bars denote 90% confidence intervals. The sample includes all SIC basins that ever host hydropower generation; outcomes are measured annually.

A.2 Tables

Table A1: Fuel properties and emission factors

Fuel	**Unit**	**Density (t/m^3)**	**NCV (GJ/unit)**	**EF (kg CO_2/GJ)**
Natural gas	m^3	–	0.038	56.1
LNG	m^3/dam^3	–	0.038	56.1
Diesel	ton / m^3	0.832	43.0	74.1
Fuel oil	ton / m^3	0.99	40.4	77.4
LPG	dam^3	–	25.3	63.1
Coal	ton	–	25.0	94.6
Petroleum coke	ton	–	31.3	97.5
Coal/petcoke mix	ton	–	30.0	95.0
Biomass	ton / m^{3}st	0.60	15.0	112.0
Black liquor	ton / m^3	0.62	13.0	93.8

Notes: Emission factors (EF) correspond to Tier 1 default values from the *2006 IPCC Guidelines for National Greenhouse Gas Inventories, Volume 2, Chapter 2*. Net Calorific Values (NCV) follow standard engineering sources. Densities are only applied when fuels are reported in volumetric rather than mass units (e.g., m^3, liters), allowing conversion to tons prior to applying NCVs. Density values come from ASTM D4052, IEA *Energy Balances*, FAO *Wood Density Database*, and TAPPI 0416.

Table A2: Distribution of First Drought Entries

Year	Hybas06	Hybas07	Hybas08	Pct06	Pct07	Pct08	Years06	Years07	Years08
Never	1	1	1						
2008	0	1	1		0.62	0.62		10.58	10.58
2012	0	2	3		0.49	0.50		6.33	6.50
2013	3	14	26	0.53	0.49	0.47	6.36	5.93	5.67
2014	1	2	2	0.46	0.52	0.52	5.08	5.75	5.75
2015	2	0	0	0.53			5.29		
2016	0	1	4		0.64	0.61		5.75	5.48
2017	5	6	7	0.55	0.55	0.57	4.42	4.42	4.52
2019	0	1	1		0.26	0.26		1.58	1.58
2020	0	0	1			0.08			0.42
2021	9	10	14	0.28	0.31	0.31	1.11	1.26	1.22
2022	0	6	17		0.32	0.39		0.97	1.16
Total basins	21	44	77						

Notes: Each cell reports (i) the number of basins (b) entering drought, (ii) the share of months in drought after entry, and (iii) the equivalent duration in years. Drought defined using the 36-month moving-window standard. "Never" indicates basins that do not enter drought during 2005–2024.

A.3 Basin-Level Drought Measurement

This appendix details our method for calculating drought conditions using runoff data across Chilean watersheds at various spatial scales. We begin with pixel-level runoff measurements, denoted as r_{pym} for pixel p in year y and month m. For each pixel, we calculate runoff anomalies as deviations from typical water availability by subtracting calendar-month averages. These pixel-level runoff data are at a spatial resolution of approximately 0.25 degrees for the entire area under study.

$$a_{pym} = r_{pym} - \frac{\sum_y r_{pym}}{Y}$$

where Y is the total number of years in our sample.

To capture the persistent nature of droughts, we compute running sums of these anomalies over the previous k months. Using period notation t for time:

$$d_{pt}(k) = \sum_{i=0}^{k-1} a_{pt-i}$$

We calculate these running sums for different windows ($k = 1, 3, 6, 9$, and 12 months), allowing us to capture both short-term fluctuations and sustained drought conditions.

To move from pixel- to basin-level measures, we use the HydroBASINS watershed database (Lehner and Grill, 2013), which provides hierarchical basin delineations from level 02 (coarsest) to level 12 (finest). As shown in Figure A10a, South America is divided into major continental watersheds at level 02, with Chile comprising a single basin along its Pacific coast. Figure A10b illustrates how our pixel-level runoff measurements are distributed across Chile on a regular 0.25-degree resolution grid. This consistent measurement grid is then integrated with basin boundaries at different scales, as demonstrated in Figures A10c, A10d, and A10e, which show basin delineations at increasing levels of detail: from 1 basin at level 02, to 167 basins at level 06, to 10,635 basins at level 12. These visualizations demonstrate how the same underlying runoff data can be aggregated at progressively finer basin resolutions. While the level 12 basin delineation provides extremely detailed watershed boundaries, it is important to note that the effective spatial resolution of our analysis is still constrained by the 0.25-degree measurement grid. Additionally, although higher resolution enables more precise basin delineation, the likelihood that we observe independent drought events in adjacent basins decreases because of the spatial autocorrelation inherent in hydroclimatic processes at these scales. For our main analysis, following previous literature (Eriksson et al., 2025), we select the level-06 basin delineation as our preferred spatial unit, as it provides an appropriate bal-

ance between geographic specificity and the spatial distribution of hydroelectric plants across the country. Figure A10f shows how plant locations (represented as points) are distributed within this basin structure. In our preferred specification, variation comes from 46 level-06 basins with power plants, out of a total of 167, capturing drought patterns from monthly variations in water availability to persistent episodes over the 2000—2024 period.

To calculate basin-level drought intensity measures, we intersect the 0.25-degree runoff data grid with the level-06 basin boundaries. For each basin b, we calculate a weighted average of the drought intensities across the intersecting pixels, using the area of intersection as the weights:

$$d_{bt}(k) = \frac{\sum_{p \in B_b} A_{bp} \cdot d_{pt}(k)}{\sum_{p \in B_b} A_{bp}}$$

where B_b is the set of pixels that intersect basin b, A_{bp} is the area of intersection between basin b and pixel p, and $d_{pt}(k)$ is the drought intensity for pixel p in time t and dimension k. This continuous basin-level drought intensity measure serves as our primary indicator in subsequent regression analyses.

Finally, we create a binary classification of drought conditions based on the basin-level drought intensity measure. Specifically, we define

$$drought_{bt} = \begin{cases} 1 & \text{if } a_{bt}^m < -\sigma\left(\{d_{bt}(k)\}_{t=1,\ldots,T}\right), \\ 0 & \text{otherwise.} \end{cases}$$

where d_{bt} is the binary drought indicator for basin b in time t, a_{bt}^m is the basin-level drought intensity measure for basin b in time t, and $\sigma(d_{bt}(k)_{t=1,\ldots,T})$ is the standard deviation of cumulative runoff anomalies over the full historical time series. This binary drought classification serves as our primary dependent variable in the subsequent regression analyses.

The methodology described above can be illustrated with time series for each step of the process. Figure A11 presents the complete analysis at different aggregations levels. The first two steps—defining anomalies and aggregating at the basin level—are illustrated in Figures A11a and A11b. Each panel shows the demeaning process by visualizing month–year series of runoff (blue line) and 1-month runoff anomalies (red line) at different spatial scales. Figure A11a presents the results for anomalies computed at the country level (i.e., at the level-02 basin level), while Figure A11b presents the results at the

finer basin level (level 06) and includes only the 46 basins that host power plants. The third step—taking running sums—is illustrated in Figures A11c and A11d, showing the running sums of the anomalies over 1, 3, 6, 9, and 12 months, with the country-level figure having a single observation and the basin-level one displaying the average across the 46 relevant basins. The last step—creating a binary drought indicator—is illustrated in Figures A11e and A11f, where the country analysis shows the presence or absence of drought conditions and the basin analysis depicts the percentage of the 46 basins with power plants that are experiencing drought.

Figure A10: Basin Delineation and Runoff Data Across Different Scales

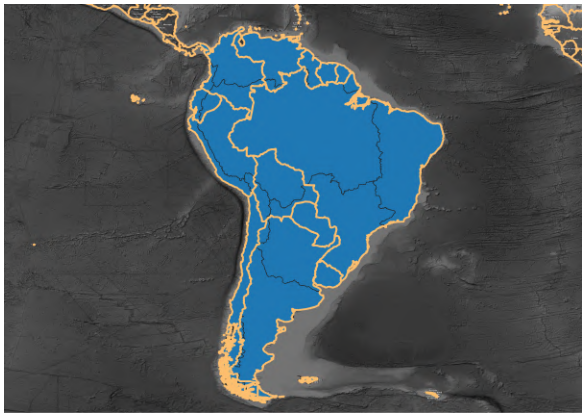

(a) Basin Boundaries (Level 02)

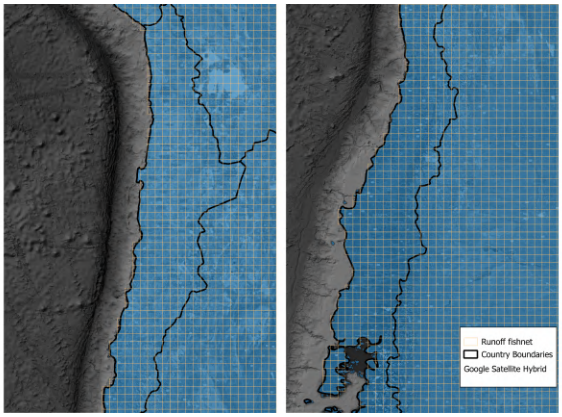

(b) Runoff Resolution: Study Area

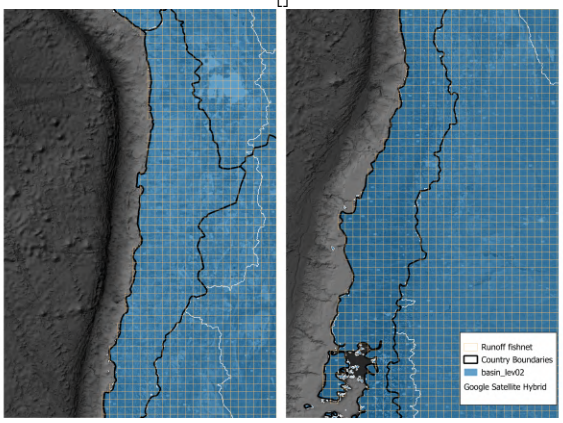

(c) Runoff Grid with Basin Level 02

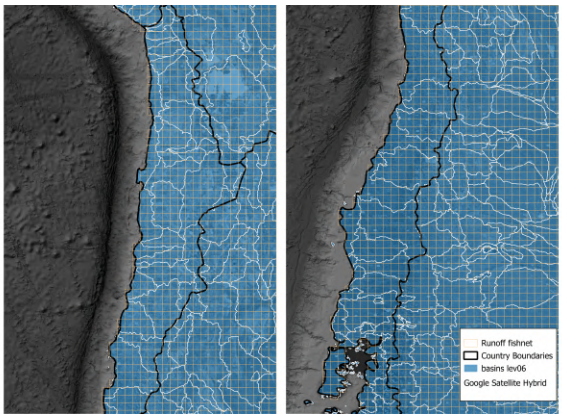

(d) Runoff Grid with Basin Level 06

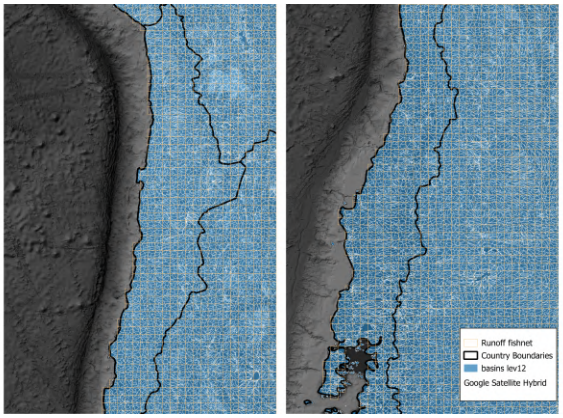

(e) Runoff Grid with Basin Level 12

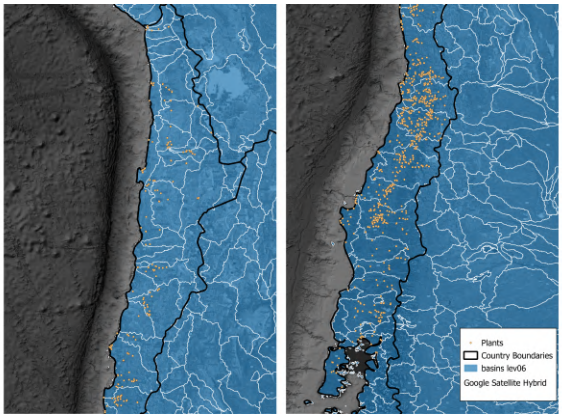

(f) Power Plants with Basin Level 06

Note: Spatial representation of the study area and basin delineation. Panel (a) shows continental-scale basins, corresponding to major watersheds across South America. Panel (b) displays the resolution of runoff data in our study area. Panels (c)–(e) illustrate the overlay between runoff data and basin delineations at increasing resolution: level 02 (national scale), level 06 (regional watershed scale), and level 12 (local watershed scale). Panel (f) shows the locations of hydroelectric power plants within level-06 basins, representing our primary unit of analysis. Level 06 provides an optimal balance between spatial resolution and meaningful aggregation for hydroelectric drought impact assessment. In our study area, level 02 closely aligns with Chile's national boundary, and we refer to level 06 as our primary basin scale in the HydroBASIN dataset (Lehner and Grill, 2013).

Figure A11: Drought Identification and Quantification at Different Basin Levels

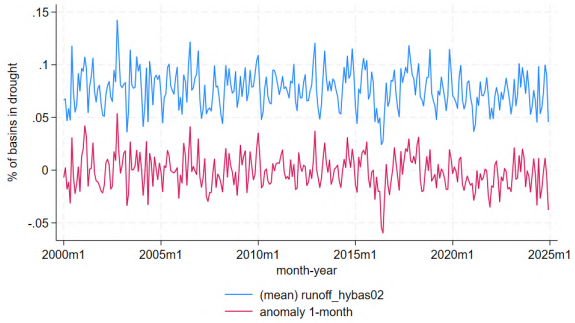

(a) Steps 1–2: Demeaned Runoff (Country-level)

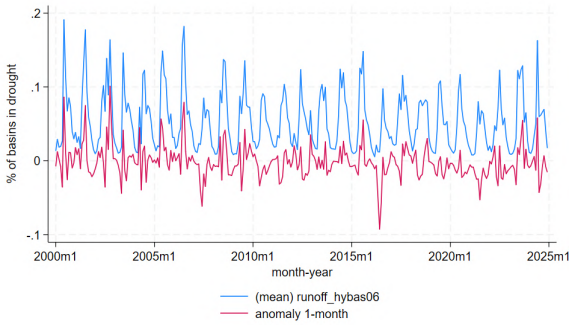

(b) Steps 1–2: Demeaned Runoff (Basin-level)

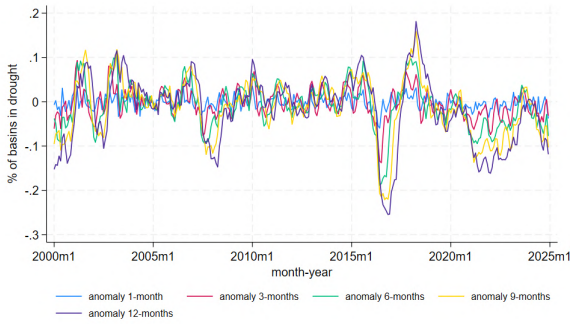

(c) Step 3: Running Sums (Country-level)

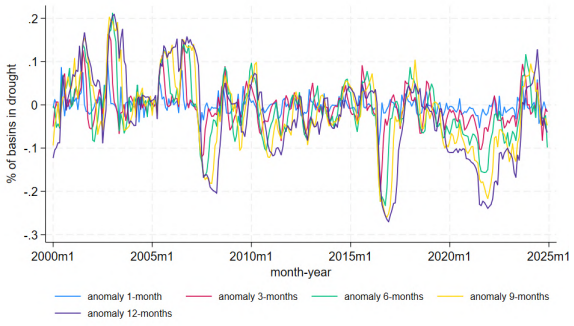

(d) Step 3: Running Sums (Basin-level)

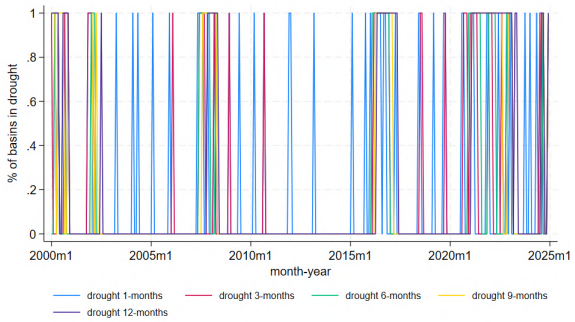

(e) Step 4: Drought Binary (Country-level)

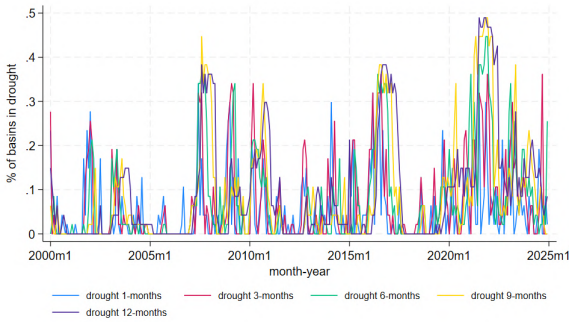

(f) Step 4: Drought Binary (Basin-level)

Note: This figure illustrates our four-step drought identification methodology. Panels (a) and (b) show Steps 1–2: monthly runoff (blue) and anomalies (red) at country level (level 02) and basin level (level 06, averaged across 46 power plant basins). Panels (c) and (d) show Step 3: running sums of anomalies over 1, 3, 6, 9, and 12 months. Panels (e) and (f) show Step 4: binary drought indicators, with the country level showing presence/absence and basin level showing percentage of affected basins. The basin-level analysis (right column) represents our preferred spatial resolution. The country level corresponds to basin level 02 (which closely aligns with Chile's national boundary), and the basin level corresponds to basin level 06 in the HydroBASIN dataset (Lehner and Grill, 2013).